Electrochimica Acta 426 (2022) 140802

Contents lists available at ScienceDirect

Electrochimica Acta

journal homepage: www.journals.elsevier.com/electrochimica-acta

Hydrothermal modification of TiO_2 nanotubes in water and alkali metal electrolytes ($LiNO_3$, $NaNO_3$, KNO_3) – Direct evidence for photocatalytic activity enhancement

Mariusz Wtulich [a,*], Mariusz Szkoda [a], Grzegorz Gajowiec [b], Kacper Jurak [c], Grzegorz Trykowski [d], Anna Lisowska-Oleksiak [a,*]

[a] Department of Chemistry and Technology of Functional Materials, Faculty of Chemistry, Gdańsk University of Technology, Gdańsk 80-233, Poland
[b] Institute of Machine Technology and Materials, Faculty of Mechanical Engineering and Ship Technology, Gdańsk University of Technology, Gdańsk 80-233, Poland
[c] Department of Electrochemistry, Corrosion and Materials Engineering, Faculty of Chemistry, Gdańsk University of Technology, Gdańsk 80-233, Poland
[d] Department of Materials Chemistry, Adsorption and Catalysis, Faculty of Chemistry, Nicolaus Copernicus University in Toruń, Toruń 87-100, Poland

ARTICLE INFO

Keywords:
TiO_2 nanotubes
Hydrothermal annealing
Redshifted VIS absorbance
Interference

ABSTRACT

The influence of hydrothermal annealing (HA) of TiO_2 nanotubes (TiO_2-NTs) in various baths (H_2O, $LiNO_3$, $NaNO_3$, KNO_3 performed for 4 h, 24 h, 64 h), on their photocatalytic and photoelectrocatalytic properties, was studied. The use of electrolytes was to enable the monitoring of photoactivity changes as a result of the expected impact on the population of hydroxyl groups on the surface. The assumption turned out to be correct and it was proved that the presence of Li^+, Na^+ or K^+ does not allow achieving the same increases in photoactivity as observed for water. Modified samples exhibit significantly decreased F, P and carbon containing species. The length of the HA annealing time considerably affected the geometry of the nanotubes: eliminated clusters, changing the tilting angle of nanotubes, the wall thickness and inter-nanotube distance. Morphology changes due to HA treatment were associated with the interference phenomenon recorded as maximum in the Vis range. HA treatment in water brings about the most photoactive and photoelectroactive material characterized with minor modification in the optical bandgap and position of the flat bad potential. The optical energy bandgap values for electrodes containing alkali metals were reduced (up to 2.72 eV) and flat-band potential was shifted towards the anodic direction (up to 0.25 V disparity). However, increased activity as photocatalysts in the methylene blue degradation process and higher photocurrent generation was achieved for samples after modification in distilled water than in electrolytes, but these parameters are still better in comparison to unmodified titania nanotubes. Long-term treatment in water and electrolytes reduced threshold potentials for oxygen evolution reaction. The studies confirmed the effectiveness of the hydrothermal method for obtaining better photocatalytic parameters of TiO_2-NTs and indicate that the presence of alkali metals is not favourable for maintaining high photocatalytic parameters.

1. Introduction

In recent decades, much work has been done on methods of controlling the morphology of TiO_2 nanotubes (TiO_2-NTs). One of the first reports, in 2001, on titania nanotubes arrays obtained by anodizing titanium foil under properly maintained conditions was published by Grimes et al. [1]. The formation of an anodically grown TiO_2 tubular structure is described in detail in Ref. [2]. It has been indicated many times that the following parameters have an enormous influence on the morphology of nanotubes in the anodization process: electrolyte composition (content of water, NH_4F, H_3PO_4 or pH) [3–5], processing time, temperature [6] and anodization potential [7,8]. Furthermore, researchers demonstrate their results on the modification of nanotubes in various ways, such as: doping with non-metals [9–11], metal doping [12–14] and building multi-component electrodes towards cascade or Z-scheme photocatalytic system [15–18] or changing morphology (single or double-wall nanotubes) [19,20]. One can find applications of different types of titanium dioxide compounds in catalysis, self-cleaning, wetting, gas sensing, interference coating, optical devices, biomedical materials (the release of drugs, implants), Li-ion batteries or

* Corresponding authors.
E-mail addresses: mariusz.wtulich@pg.edu.pl (M. Wtulich), alo@pg.edu.pl (A. Lisowska-Oleksiak).

https://doi.org/10.1016/j.electacta.2022.140802
Received 28 April 2022; Received in revised form 1 July 2022; Accepted 2 July 2022
Available online 4 July 2022

supercapacitors [2,21–25]. Moreover, there is an increasing importance of nanomaterials in the design of solar cells and photocatalytic devices for environmental protection. This applies to both the production of so-called solar fuels and the removal of organic pollutants from water and air. All applications related to photocatalysis and photoelectrocatalysis focus on geometric [26,27], optical [28,29] and electrochemical properties [30] in conjunction with the morphology and electronic structure of TiO_2 nanotubes.

A little-known method of anodically produced nanotubes is their modification using hydrothermal annealing (HA). The first study devoted to the testing effect of HA on the photocatalytic properties of anodized TiO_2 was described by Yu et al. [31]. The work shows that amorphous nanotubes hydrothermally treated in autoclaves lead to aggregation of TiO_2 into particles. Subsequent similar works [32–36] show the dissolution and anatase recrystallization of amorphous TiO_2 by water annealing (also known as the water-soaking method). These tests were carried out under atmospheric pressure.

The only report that showed the effect of hydrothermal modification in an autoclave on calcined TiO_2-NTs under increased pressure is reported in Ref. [37]. However, after annealing titania nanotubes were finally calcined after HA. To our knowledge, no one focused on the effect of HA on calcined titania nanotubes without subsequent calculations.

Therefore, in this study, the influence of hydrothermal annealing process time and the bath composition (H_2O, $LiNO_3$, $NaNO_3$, KNO_3) for HA modification of TiO_2 nanotubes on the morphology, elemental composition, photoelectrocatalytic activity towards water oxidation and the photocatalytic degradation of methylene blue (MB) were tested. Tests in the presence of alkali metal cations were undertaken as cations may modify –OH groups' surface population and have an impact on photocatalytic activity of hydrothermally modified anodized titania nanotubes.

Here changes in optical, electrochemical, photoelectrochemical and photocatalytic properties are evaluated to hydrothermal procedure conditions. Samples have been characterised using scanning electron microscopy (SEM), X-ray photoelectron spectroscopy (XPS), X-ray powder diffraction (XRD) and UV-Vis spectroscopy. All electrodes were tested using cyclic voltammetry (CV), linear sweep voltammetry (LSV), electrochemical impedance spectroscopy (EIS) in the dark and chronoamperometry (CA) under solar light illumination.

2. Experimental

2.1. Materials

Chemical reagents used in the anodization process, HA modification, electrochemical and photocatalytic process were of analytical grade: NH_4F, ethylene glycol were purchased from Chempur (Piekary Śląskie, Poland); H_3PO_4, $NaNO_3$, KNO_3 were purchased from POCH Gliwice (Gliwice, Poland); $LiNO_3$, K_2SO_4 and methylene blue were purchased from Sigma-Aldrich (St. Louis, USA). Alfa Aesar (Kandel, Germany) provided titanium foil (99.5% metals basis, annealed, thickness 0.25 mm). In all studies, triple distilled water was used. The electrical conductivity of triple distilled water is $1.5{\cdot}10^{-6}$ S cm^{-1}.

2.2. Preparation of the electrode materials

The titanium foil was cut into thin 2×2 cm^2 squares and subjected to pressing with a force of 2 tons. Samples were degreased in an ultrasonic bath in a 1:1 solution of acetone and isopropyl alcohol for 20 min at 40°C, then rinsed in water. Next, both metal plates were placed for anodization in a two-electrode glassy cell keeping the 2 cm distance between the anode and cathode plates. One compartment, thermostated cell was filled with the 100 ml solution of an ethylene glycol electrolyte containing: 1 g NH_4F, 5 ml H_2O and 3.5 ml H_3PO_4 [13] to obtain titania nanotubes. TiO_2-NTs were synthesized at the constant voltage of 40 V for 2 h, keeping the temperature at 20 ± 1°C. Beyond thoroughly rinsing, the samples were calcined in a furnace at 450°C (the rate of heating – 2.5°C/min) with airflow and cooled down in air at room temperature after 2 h of heating. The final step was to transfer electrodes to an autoclave equipped with a PTFE-lined stainless steel chamber for further HA at 100°C (30 ml electrolyte per 50 ml total chamber volume). This modification was performed at different times (4, 24 and 64 h) and various solutions (a triple distilled water, an aqueous electrolyte of 0.15 M $LiNO_3$, 0.15 M KNO_3, 0.15 M KNO_3).

2.3. Materials characterization

The electrode morphologies were characterized by JSM-7800 F (JEOL, Tokyo, Japan) field emission scanning electron microscope. The microscopic studies were analyzed using a beam accelerating voltage at 5 kV. Energy-dispersive X-ray spectroscopy (EDX) was used to identify chemical elements by a silicon nitride window's detector (OCTANE ELITE model, EDAX company, New Jersey, USA). The technique for measuring the intensity of discrete wavelengths in the range 200 ÷ 800 nm was provided by UV-Vis spectroscopy, using the Perkin Elmer UV-Vis spectrometer (Lambda 35, Perkin Elmer, Waltham, MA, USA) equipped with the integrating sphere module to estimate the reflection of the measurements. X-ray powder diffraction was used to determine the crystal structure of the obtained TiO_2 samples. Measurements were made using a diffractometer (Xpert PRO-MPD, Philips, Amsterdam, Netherlands). X-ray photoelectron spectroscopy measurements were performed on the Escalab 250Xi device (Thermo Fisher Scientific, Waltham, Massachusetts, USA) with Al Kα radiation and pass energy. The analysis and deconvolution of the spectrum of the elements were described using a Gaussian–Lorentzian sum envelope with an asymmetry tail supported by commercial Avantage version 5.973 spectrometer software [38]. All of the binding energies obtained in the XPS were calibrated by the C1s line at 284.8 eV. The spot width with a diameter of 650 μm was used. The electrochemical and photoelectrochemical measurements of titania nanotubes were carried out with a potentiostat–galvanostat (Autolab PGSTAT 30, Metrohm Autolab B.V. and AutolabPGStat10 with an FRA module, Eco Chemie B.V both from Utrecht, Netherlands) in a three-electrode cell: TiO_2-NTs (active surface area of 0.7 ± 0.1 cm^2) as the working electrode (WE), a platinum mesh as the counter electrode (CE) and Ag/AgCl/0.1 M KCl as the reference electrode (RE). Linear sweep voltammetry, cyclic voltammetry, chronoamperometry and electrochemical impedance spectroscopy were conducted in water-based solution electrolyte (0.1 M K_2SO_4) purged with argon (Ar gas high purity, O_2<0.2 ppm) for half an hour before measurements. The temperature was kept constant (20 ± 1°C) with a thermostat (Julabo F-12, Seelbach, Germany) in all measurements. The flat band (E_{fb}) potentials were determined using EIS. Frequencies were measured from 20 kHz to 1 Hz for 10 points per decade with low amplitude (10 mV point-to-point) of the AC signal. Photoelectrochemical studies were conducted in a three-electrode glassy cell with a quartz window. The tested electrodes remained in the same electrolyte and under the conditions described above. Solar lighting was a xenon lamp (Osram XBO 150, Quantum Design, Darmstadt, Germany), which generates light with an intensity of up to 100 mW/cm^2, equipped with an air mass 1.5 filter and an automatic shutter that opens/closes every 5 s. The studies on the influence of TiO_2-NTs on the degradation of methylene blue were carried out in a dark glass reactor, isolated from external light. The photocatalytic reactions were conducted in a 50 ml water-based solution of 10^{-5} M methylene blue (MB) under illumination using the lamp described above. The decomposition of the MB was recorded every 30 min using the UV-vis spectrophotometer (model UV5100, METASH). The current MB concentration was registered as an absorbance measurement at $\lambda = 665$ nm. For reference, a blank test was performed under the same conditions but without TiO_2-NTs.

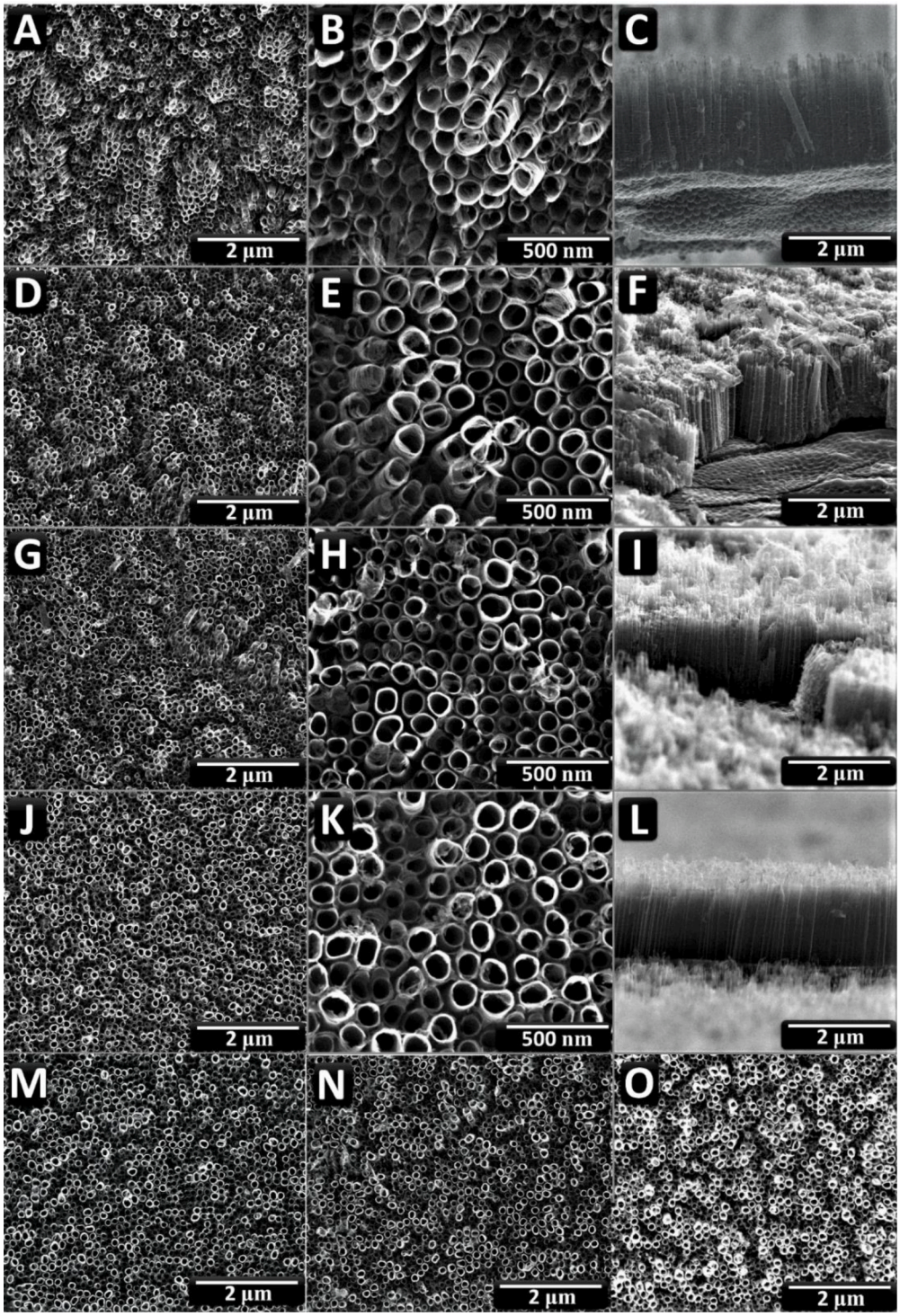

Fig. 1. Top-view SEM images at 10k, 100k magnification and cross-section images at 10k magnification respectively for: (A–C) unmodified TiO_2-NTs; HA TiO_2-NTs in water for (D–F) 4 h, (G–I) 24 h, (J–L) 64 h and top-view SEM images at 10k magnification for HA TiO_2-NTs in an electrolyte of 0.15 M (M) $LiNO_3$, (N) $NaNO_3$, (O) KNO_3 for 64 h.

3. Results and discussion

3.1. Morphology and composition of the samples

3.1.1. Scanning electron microscope imaging

Fig. 1 A–O show SEM images of the top-view and cross-sectional images of the: (1A-C) TiO_2-NTs - calcined, (1D-F) TiO_2-NTs after hydrothermal annealing in water for 4 h, (1G-I) for 24 h and (1J-L) for 64 h and TiO_2-NTs after HA in an aqueous solution of 0.15 M (1M) $LiNO_3$, (1N) $NaNO_3$, (1O) KNO_3 for 64 h. All obtained nanotubes have a single-wall structure. As shown in Fig. 1A, the electrode surface consists of titania nanotubes agglomerated into small local clusters. At higher magnification (Fig. 1B), it can be seen that such one cluster is created of a dozen interconnected nanotubes by their walls. Some upper parts edges of the nanotubes touch each other and look like to be stratified, jagged and inhomogeneous. The average inner nanotubes diameter is 99

Table 1
Data obtained from geometrical analysis of SEM images (Fig. 1), where h –the length of the nanotube, R_1 – is the internal radius, R_2 – a distance between the nanotube centre and the centre of the nanotube wall, y – a distance between neighbouring nanotubes, w – a thickness of nanotube, S_t – a total developed surface.

Sample	*h* (nm)	$2{\cdot}R_1$ (nm)	R_2 (nm)	*y* (nm)	*w* (nm)	S_t (cm^2)
TiO_2-NTs	1882 ± 52	99 ± 9	58 ± 5	10 ± 4	10 ± 3	86.6 ± 9.7
in H_2O, 4 h	1556 ± 93	102 ± 11	60 ± 5	20 ± 3	17 ± 4	54.6 ± 10.5
in H_2O, 24 h	1556 ± 94	102 ± 9	56 ± 6	21 ± 3	14 ± 3	58.4 ± 9.6
in H_2O, 64 h	1522 ± 82	107 ± 12	60 ± 5	23 ± 3	19 ± 6	50.5 ± 9.5

± 9 nm and the length is 1882 ± 52 nm (estimated from 15 counts from Fig. 1B and C). In Fig. 1D, one can still see clusters of nanotubes. However, when enlarged (Fig. 1E), it can be seen that nanotubes have been separated, they do not touch their walls. The significant change is the diminution of the thickness of the nanotube layer to 1556 ± 93 nm (Fig. 1F). It is well known that nanotubes are conical [39]. The diminution in length is very likely to be caused by the etching of parts of the nanotubes at the thinnest or stratified places. During HA in water, molecules of H_2O and residual fluoride anions [40], can etch the TiO_2-NTs via $[TiF_6]^{2-}$ soluble complex formation. The view of the more homogeneous nanotubes than unmodified TiO_2-NTs is depicted in Fig. 1G and J. Titania nanotubes were separated and no clusters are present. The enlarged shows that the nanotubes do not touch each other edges of the neighbouring walls (Fig. 1H and K) as well as TiO_2-NTs HA in water (4 h). Additionally, they were straightened after the hydrothermal annealing for a longer time (24 h, 64 h). This suggests that possibly the long term HA decreased residual stresses and complete relaxation occurring during this process, as can be seen on the XRD diffractogram, see paragraph 3.1.2 The inner diameter and the length of these TiO_2-NTs are similar and collected in Table 1. The top-view images of TiO_2-NTs HA in electrolytes (Fig. 1M–O) show that the morphology of the electrodes is very similar in comparison to titania nanotubes hydrothermally annealed in water for 64 h.

Table 1 shows the geometric parameters (symbols are the same as given in Ref. [41]) that are important to optimize the TiO_2-NTs morphology, thanks to which the electrode material shows better photoactivity. Although the TiO_2-NTs calcined layer (before HA) was thicker, the morphology was heterogeneous (inclined, stratified nanotubes preventing light from propagating deep into), which may result in lower photocurrent being generated [42].

As shown in the literature [43], the efficiency of a solar cell strongly depends on its morphology. The open tube tops have a significant advantage in this system. The condition of the surface for any catalytic processes is of great importance [44]. Therefore, not only in the morphological changes, the cause of the increase in photoactivity should be sought, but also in the chemical state of the surface, so it is presented below.

Table 2
Elemental content (at. %) of TiO_2-NTs before and after hydrothermal annealing was detected by EDX.

Sample	TiO_2-NTs	in H_2O			in $LiNO_3$			in $NaNO_3$			in KNO_3		
		4 h	24 h	64 h	4 h	24 h	64 h	4 h	24 h	64 h	4 h	24 h	64 h
Ti (at. %)	41.50	42.53	43.06	46.26	44.88	43.22	42.58	46.67	44.23	41.54	37.25	42.87	46.96
O (at. %)	56.92	56.72	56.09	53.06	54.45	55.98	56.45	52.68	54.70	57.48	60.97	56.25	52.27
F (at. %)	0.99	0.56	0.56	0.54	0.59	0.57	0.57	0.46	0.91	0.83	0.68	0.65	0.59
P (at. %)	0.59	0.19	0.29	0.14	0.23	0.23	0.23	0.19	0.16	0.15	0.23	0.23	0.18

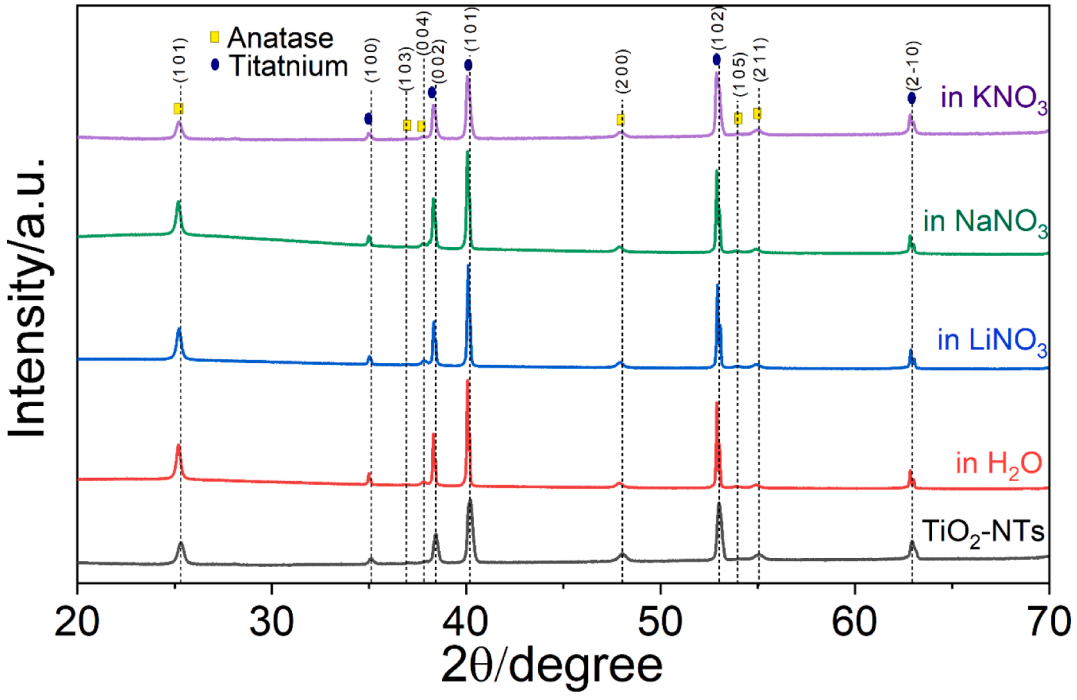

Fig. 2. Comparison of XRD patterns of TiO_2-NTs before and after hydrothermal annealing in water $LiNO_3$, $NaNO_3$, KNO_3 (64h).

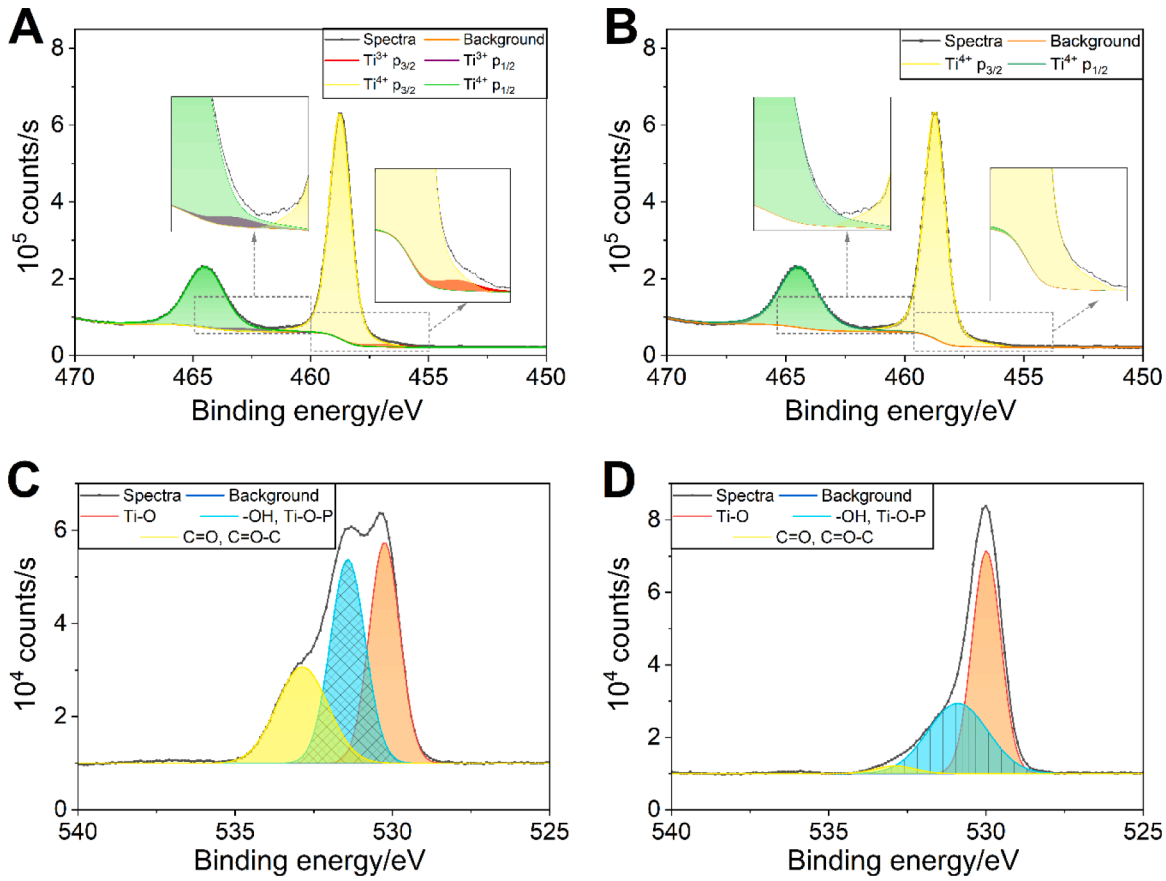

Fig. 3. Deconvolution of titanium 2p peak in the XPS spectra of TiO_2-NTs after HA for 24 h in water in the: (A) presences of Ti^{4+} and Ti^{3+} (B) presences only Ti^{4+}; and oxygen 1s peak for TiO_2-NTs (C) before and (D) after treatment (H_2O, 24 h).

3.1.2. *Energy dispersive X-ray analysis*

EDX measurements were performed to determine the atomic percentages of the elements: titanium, oxygen, as well as the contamination of fluorine and phosphorus, obtained by the anodization of Ti foil as described earlier [13]. It is known that the calcination of the as-formed nanotubes removes the fluorine ions due to the evaporation of gases such as F_2 and HF [45]. However, a small residual content of fluoride ions, less than 1 at. %, remains in the structure of the calcined TiO_2 nanotubes. Table 2 shows that the sample after the HA in water contains a significantly lower amount of F (almost twice) and P (fourfold). Moreover, the content of phosphorus in the samples subjected to HA in all electrolytes was reduced at least 2.5 times. Except for the sample modified in an aqueous electrolyte $NaNO_3$, a tendency was noticed that the HA eliminates the residual elements after anodization. It can be concluded that the HA method reduces the content of impurities in the form of fluoride and phosphorous. As the authors write in Ref. [36], for the sample subjected to a 3-day water annealing at 70°C, the content of the elements is: 51.79% for O, 46.09% for Ti and 0.09% for F, which is comparable with the result obtained for TiO_2-NTs in H_2O 64 h from this work. In particular, they show that fluoride residues are removed by a longer water annealing time of the nanotubes by leaching out. However, water-soaking requires a longer time to achieve the same results as HA in our work.

3.1.3. *XRD*

Crystallinity and phase composition of TiO_2-NTs: unmodified, hydrothermally annealed in water and 0.15 M aqueous solution of $LiNO_3$, $NaNO_3$, KNO_3 for 64 h was measured by XRD. Fig. 2 shows the registered diffraction at 25.2^O, 36.9^O, 37.8^O, 38.6^O, 47.9^O, 53.9^O, 54.9^O which correspond to the (1 0 1), (1 0 3), (0 0 4), (2 0 0), (1 0 5), (2 1 1) planes, respectively [46]. All electrodes are composed of the anatase phase. No reflections referring to rutile or brookite were recognized. The observed signal at 35.0^O, 38.3^O, 40.1^O, 52.9^O, 52.9° correlate to Miller indices (1 0 0), (0 0 2), (1 0 1), (1 0 2), (2 -1 0) of HCP crystal structure of titanium [47]. The highest intensity reflections correspond to Ti planes because it is the main electrode material. No additional differences were detected in the changes in the XRD pattern for the tested samples. However, for HA of TiO_2-NTs, a slight shift and less broadening of the peaks with reflections corresponding to the anatase planes are observed. This may mean that the quantitative residual stresses (microstrains) and the size of the crystallites have decreased compared to the pure titania nanotubes [48–50]. One could expect traces of rutile at the bottom of the tubes [51], but in our case, XRD patterns show only the anatase phase in all cases, which is consistent with XRD data of TiO_2-NTs calcined at 450°C [52].

3.1.4. *X-ray photoelectron spectroscopy*

The Ti2p spectra are very similar for all samples, regardless of the electrolyte used in HA, composition and the annealing time. Minor discrepancies at the level of 0.1–0.2 eV are due to the accuracy of the measuring device and the accuracy of the calibration based on C1s. The observation of all XPS spectra for the HA modified (12 pieces) and the unmodified samples allows distinguishing qualitative differences (insignificant) in the course of the curves, see Fig. S1. A slight broadening is observed at the base of the Ti (IV) peak at about 460 eV. The observed broadening disappears for all the modified electrodes. This change occurs regardless of the type of hydrothermal bath. Moreover, all modified samples are characterized by a narrower XPS spectrum at maximum ($Ti^{4+}p_{3/2}$) compared to the original, unmodified TiO_2-NTs. This widening at the bottom, which disappears with all other HA

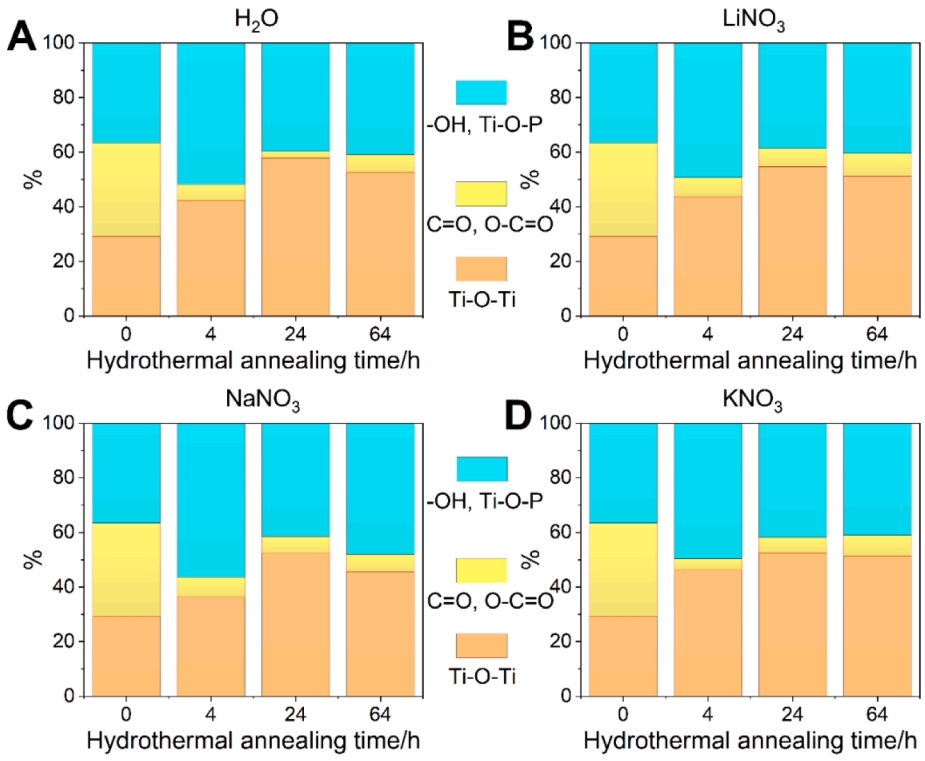

Fig. 4. XPS spectra of O 1s for TiO_2-NTs before and after hydrothermal annealing in (A) water, (B) 0.15 M $LiNO_3$, (C) 0.15 M $NaNO_3$, (D) 0.15 M KNO_3. Spectra are narrowing with HA.

modified samples, may indicate that the surrounding area of the Ti (IV) ion is altered as a result of the hydrothermal process. A model for the Ti2p analysis was proposed, taking into account the simultaneous occurrence of Ti^{4+} and Ti^{3+}. After analysing all spectra, the Ti^{3+} content was estimated at 0.5–2.5% (Fig. 3A). There was no dependence of the percentage of this form of titanium on the electrolyte composition or the length of the annealing. Since the presumed Ti^{3+} content is very low, a model with Ti^{4+} only was proposed (Fig. 3B). Powell fitting algorithm and Gaussian-Lorentzian Convolution were used. In both models, the Ti^{4+} $2p_{3/2}$ peak appears at BE around 458.8 eV and the Ti^{4+} $2p_{1/2}$ peak at BE around 464.5 eV. The splitting between these peaks equals 5.7 eV which is consistent with the literature [53] and corresponds to TiO_2 lattice structure (O^{2-} is coordinated Ti^{4+} in the tetragonal phase of anatase) [54]. Ti^{3+} shows the best match for BE at around 457 eV, which is also in line with the literature. Normalized Chi Sqr for the model without Ti^{3+} was 7.1148 with 3 iterations, and for the model with two forms of titanium was 4.8314 with 8 iterations. Detecting a negligible amount of Ti^{3+} on a Ti^{4+} background is not easy and the measurement

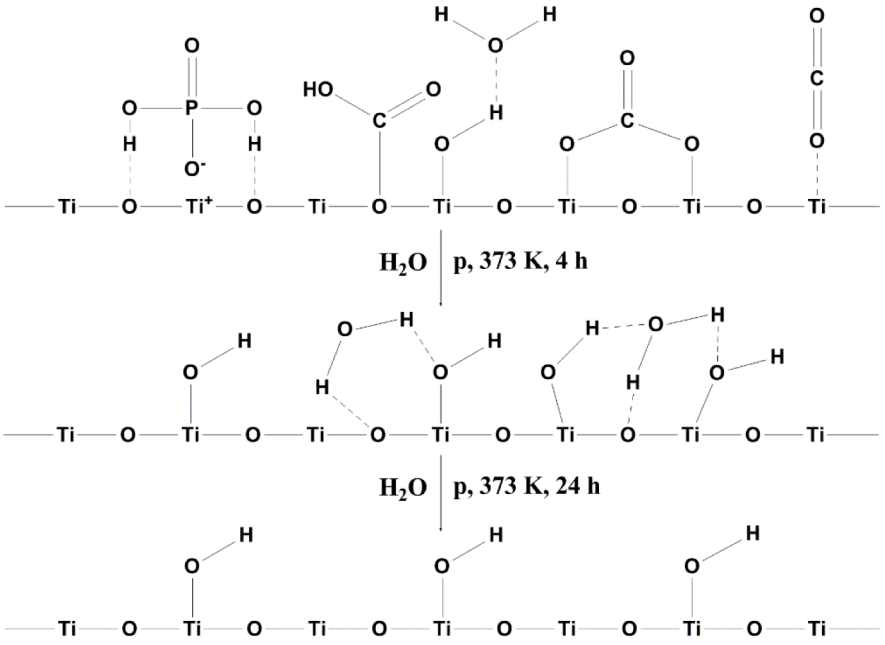

Fig. 5. Possible surface structures on the TiO_2-NTs surface for calcined and hydrothermal annealed samples.

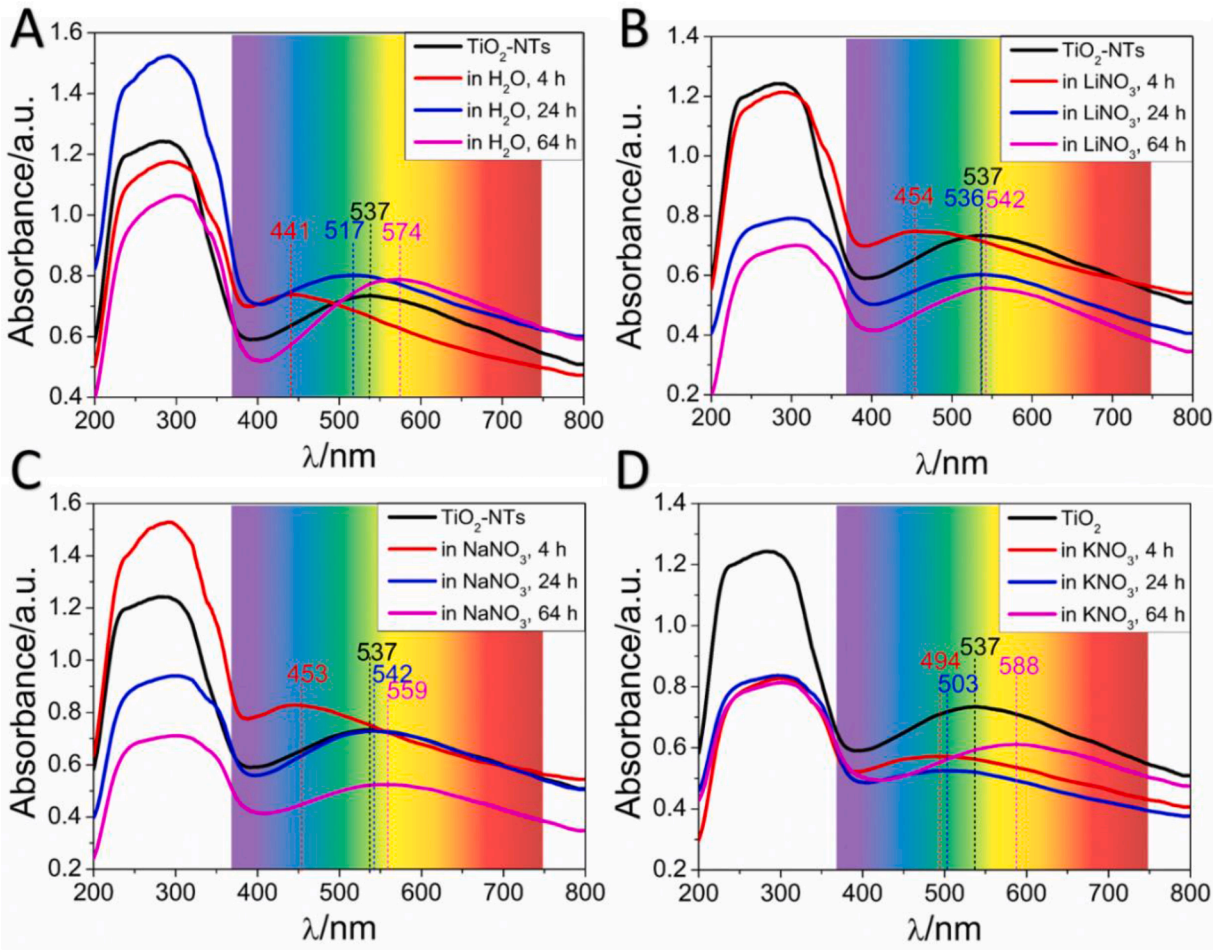

Fig. 6. Absorbance spectra for TiO_2-NTs after hydrothermal annealing in: (A) water, (B) in 0.15 M $LiNO_3$, (C) in 0.15 M $NaNO_3$, (D) in 0.15 M KNO_3.

capabilities of the device are limited. When analysing such small contents, high measurement accuracy is needed, hence the models assuming the presence of Ti^{3+} and its absence match at a similar level and in assessing the presence of titanium forms, additional measurement methods should be used.

Fig. 3C shows the deconvolution of the XPS spectrum to the O 1s peak, with the resolution of three main signals for TiO_2-NTs electrode. The first peak is localized at 530.2 eV and is attributed to the oxygen state of the TiO_2 lattice (octahedral TiO_6 formed by atoms O^{2-}-Ti^{4+}) [31,55]. The second peak at 531.4 eV has the biggest share in the distribution of the oxygen spectrum (36.57%) and can be assigned to the surface -OH and TiO_x species [56] or the oxygen atoms in the phosphonate group (Ti-O-P, O=P) [54,57]. The last signal localized at a binding energy of 532.8 eV corresponds to carbon-containing groups (O=C-O, C=O) [58], physically absorbed H_2O [31] on the near-surface area or C-OH [59], P-OH [57] bonds.

For all XPS spectra of O 1s for TiO_2-NTs after HA in H_2O, $LiNO_3$, $NaNO_3$ and KNO_3 see Fig. S2. Fig. 3D depicts the deconvolution of the oxygen of TiO_2-NTs HA in water for 24 h. It can be seen that the peak (O1s at 530.0 eV) attributed to Ti-O-Ti bond is more intense. The signal O 1s at 532.8 eV is significantly lower than for the electrode before HA. The third O1s signal from carboxylate is detectable in the range of error. The detailed distributions of oxygen towards the HA time for all electrodes are shown in Fig. 4. Regardless of the choice of water or electrolyte for hydrothermal modification, after 4 h of HA, a significant drop in the peak contribution O 1s at the highest 532.8 eV binding energy can be seen, in Fig. 3 and Fig. 4. The reason for this is most likely the fact that carbon-containing groups (firstly present due to anodization in glycol electrolyte) are leached out during HA.

Fig. S3 shows all XPS spectra of C 1s. For each electrode subjected to hydrothermal modification in water and electrolytes, spectra showing decreased intensities were recorded (lower carbon content) for modified samples, which is generally in accordance with changes of oxygen content. Fig. S4 shows the deconvolution of carbon 1s peak for TiO_2-NTs HA in water. It can be seen that HA leads to leach out the C=O and O=C-OH groups attributed at binding energies of 287.6 eV and 289.2 eV, respectively [59]. After 24 h, these signals disappear and a new one appears at the energy of 288.6 eV, which is assigned to the HCO_3^- group [60]. This change may be attributed to the surface chemical reaction between carbon near-surface species and water resulting in HCO_3^- formation, see a green hump in Fig. S4. These changes of carbon species content are consistent with those observed for the XPS spectra of O 1s in Figs. S2 and 4.

Notwithstanding, at higher temperatures and under increased pressure, various changes in surface chemistry are expected to occur. Fig. 5 shows possible changes in the TiO_2-NTs surface during HA. The remaining adsorbed water could have undergone various surface adsorption processes. With increasing time of treatment, different species on TiO_2-NTs surface stabilize by the hydrogen bonds with adjacent anions, which are described in more detail in Ref. [61]. We see this as the highest proportion of oxygen (over 50%) for the peak at the binding energy of 530.8 ± 0.1 eV. Moreover, it differs from the O1s from an unmodified sample by as much as 0.5 ± 0.1 eV. This can be explained by the removal of the phosphate groups during HA, as shown in Figs. S5 and S6.

Hydrothermal annealing caused the oxygen content to drop at the O 1s 530.8 ± 0.1 eV (Ti-OH) peak and increase at O 1s 529.9 ± 0.1 eV (Ti-O-Ti). This was probably due to the chemical reaction taking place on

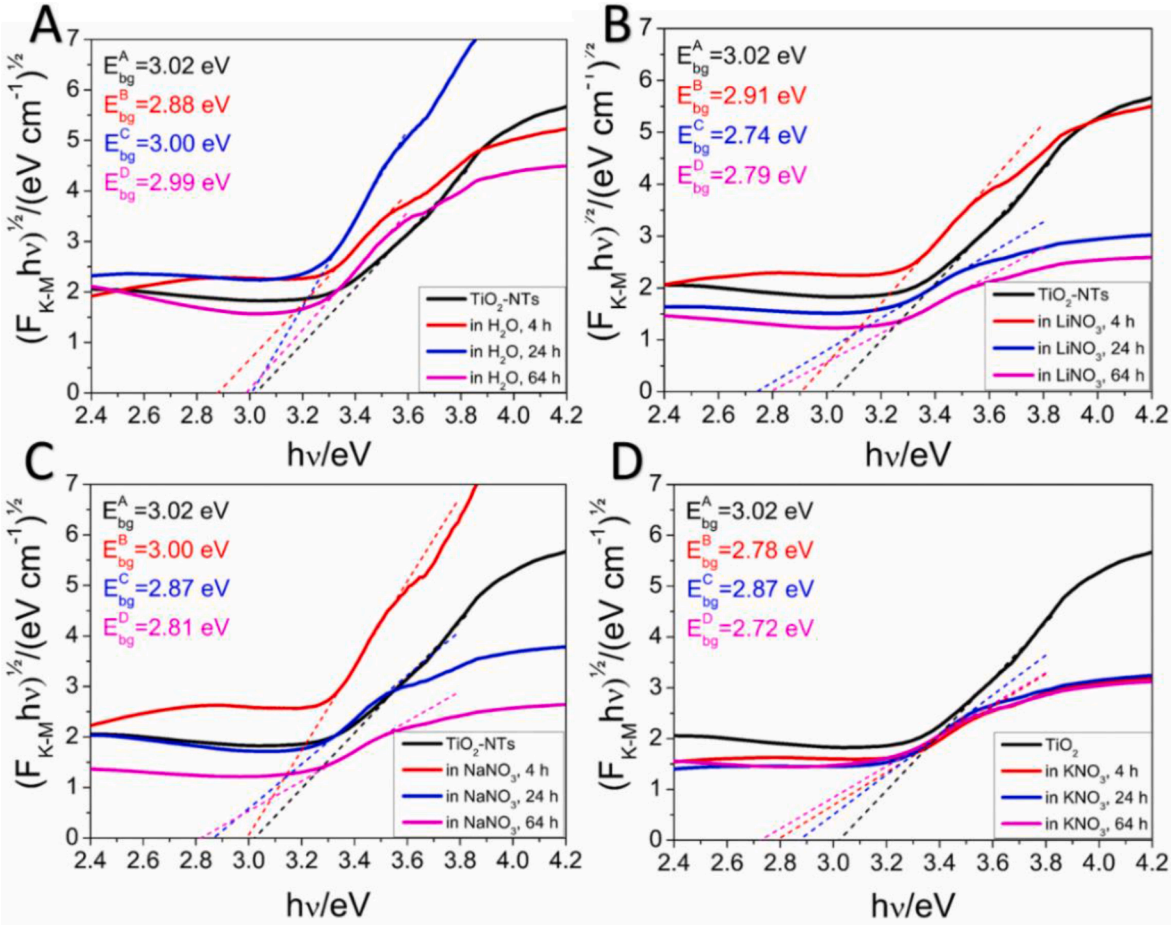

Fig. 7. Tauc plot for TiO_2-NTs after hydrothermal annealing in: (A) water, (B) in 0.15 M $LiNO_3$, (C) in 0.15 M $NaNO_3$, (D) in 0.15 M KNO_3.

the TiO_2-NTs surface during the hydrothermal process, given by the equation below [62]:

$$Ti-OH+OH-Ti \xrightarrow{T,\ p} Ti-O-Ti+H_2O \quad (1)$$

The content of hydroxyl groups is crucial in the context of photocatalytic properties [62,63]. The following hours of HA do not show a significant change in the content of individual bonds with oxygen. However, it can be assumed that titanates of the Ti-O-Me structure (where Me is: Li, Na or K) may be formed [64,65], within the measurement error influencing the surface hydrogen groups population.

$$Ti-OH+Me^+ \rightarrow Ti-O-Me+H^+ \quad (2)$$

Besides, as shown in Fig. S7, small amounts of potassium or sodium, but not light lithium, were detected on the TiO_2-NTs near surface. All of the above elements were in small amounts (up to at. 1,5%). No fluoride was detected on the surface of any samples measured by XPS. On the other hand, according to EDX studies, which reveal a low content of fluorine in the electrode (per volume), probably most of the fluoride accumulates within the bulk of the nanotubes (most at the bottom – F^- rich layer) [43]. According to reaction (1), hydrothermally treated TiO_2 surface can adsorb H_2O molecule effectively on Ti centre. Subsequent hydrogen bonding with O centre may result in H_2O dissociation – influencing the catalytic activity of the oxide surface [44]. Thus, samples with higher content of oxygen from Ti-O-Ti are expected to present higher catalytic activity as observed.

3.2. *UV-vis spectroscopy*

It is known from the literature that spectra in the UV-vis range for titanium dioxide nanotubes usually have two well-formed, wide absorption maxima, one in the UV range and the other in the Vis range. Fig. 6A–D shows the UV-vis spectra, illustrating the absorbance curves for TiO_2-NTs before and after HA. The highest absorbance maxima, typical for TiO_2 in the crystal structure of anatase and determining bandgap energy E_{bg} are in the range of ultraviolet. The absorption spectra were used to determine the E_{bg} value (see the next paragraph). Hydrothermal modification leads to an increase in absorption under optimal conditions for each system. And so, for the electrode modified in water, the highest values were obtained after 24 h of HA (Fig. S8A). The factors influencing the change in absorption in the UV region are the change in the geometry of the TiO_2-NT layers and the removal of carbon-containing groups such as C=O, C-O=C, F, O-P, see XPS data, Figs. 5, S3 and S6. The influences of these factors are opposite. Observed changes in geometry over time lower the absorption, while the removal of pollutants influences its growth. Moreover, the share of alkali metal cations tends rather lower the absorption of UV light due to alkali metal cations' insertion into the near-surface area, probably in a form of titanates.

The analysis of the absorbance spectrum in the VIS range shows a certain trend in the position of the maximum related to treatment time. In the first period of HA (up to 4h), the maximum shifts towards higher energies, as blueshift is observed. Regardless of the medium contained in the hydrothermal bath, the maximum absorbance values of TiO_2-NTs are in the region of blue light. Further extending the modification time results in a shift of the peak in the visible range into the area of lower energy, so we observed a redshift. For samples after 24 and 64 h of treatment, the maximum is in the range of green and yellow light, respectively. This trend is notably visible in Fig. 6A. The reason for these changes in the position of the wide maximum in the Vis range can be

Table 3
Flat band potentials estimated from impedance function measured at 1000 Hz vs Ag/AgCl 0.1 KCl reference electrode.

Sample	TiO_2-NTs	in H_2O			in $LiNO_3$			in $NaNO_3$			in KNO_3		
		4 h	24 h	64 h	4 h	24 h	64 h	4 h	24 h	64 h	4 h	24 h	64 h
E_{fb} (V)	-0.25	-0.18	-0.05	-0.15	-0.23	-0.17	-0.05	-0.06	-0.09	-0.07	-0.18	-0.18	0.00

found in two areas, namely: (a) in changes in the electronic properties of the area near the surface and (b) in changes resulting from the geometry of the sample and in the interference phenomenon due to thin-film optical properties.

The first reason is that changes in such a spectrum may correspond to self-trapped excitons, oxygen vacancies (OVs) and surface states [66]. According to the literature, the most intense signal of unmodified TiO_2 is associated with the presence of fluorine and phosphorus [67]. Diminishing the atomic content of F and P can change the energy of the electron transitions and the self-trapped excitons, resulting in the higher absorption of shorter wavelength light, which is seen as a blueshift for all samples after 4 h of HA [68,69]. However, the major factor responsible for redshift may be the oxygen vacancy occupied by one or two electrons [70]. Moreover, as reported in the literature [71], higher Ti^{3+} content causes the absorbance curve to shift towards longer wavelengths in the Vis range. As shown in Fig. 3A, the presented model of the deconvolution of the XPS spectrum shows a low presence of Ti^{3+}. For this reason, it cannot be excluded that the presence of Ti^{3+} is responsible for the peak in that Vis region. Slight differences in the maximum absorbance shift may result from the insertion of alkali metal ions to the TiO_2-NTs surface area as proven by XPS.

The second reason, but the most prominent, explaining the change in the absorbed wavelength of light in Vis region, is based on the theory of interference phenomenon (Fabry–Pérot interference) [72]. As reported in the works [73,74], the local maximum value of the Vis spectrum depends on the thickness of the obtained TiO_2 layer, which corresponds to a specific colour. As it turns out, for all TiO_2-NTs (calcined and HA), the key role in the absorbance measurement in Vis region is their geometry, especially: diameter, thickness and length of the nanotube, intertube distance and wall structure [35,75]. Moreover, the higher the tilting angle of titania nanotubes to the surface, the local maximum shifts towards the UV range, as shown by the numerical calculations [35]. Our work shows that HA causes an increase in the wall thickness of TiO_2-NTs and reduces the angle of inclination of TiO_2-NTs to titanium substrate and the length of nanotubes, see SEM images Fig. 1. According to the conditions of wave interference and the results discussed above, it could be confirmed that the trend in the position of maximum in Vis region spectrum is caused by changes in morphology.

Considering the above, we show that the change in the local maximum absorbance of titania nanotubes in visible light has two kinds of grounds – electronic states and geometry of TiO_2-NTs able to produce interferential colours [35].

Using the absorbance spectra and the Kubelka-Munk function, the values of bandgap energy (E_{bg}) were determined for all obtained materials based on the Tauc plot, which is presented in Fig. 7A–D. Hydrothermal modification of titania nanotubes in water did not change the E_{bg} value, except for negligible change for sample TiO_2-NTs in H_2O (4h). The samples hydrothermally annealed with alkali metal electrolytes exhibited lower values of the bandgap energy. As noted above, TiO_2-NTs in KNO_3 (64h) exhibits the smallest value of E_{bg} and equal 2.72 eV.

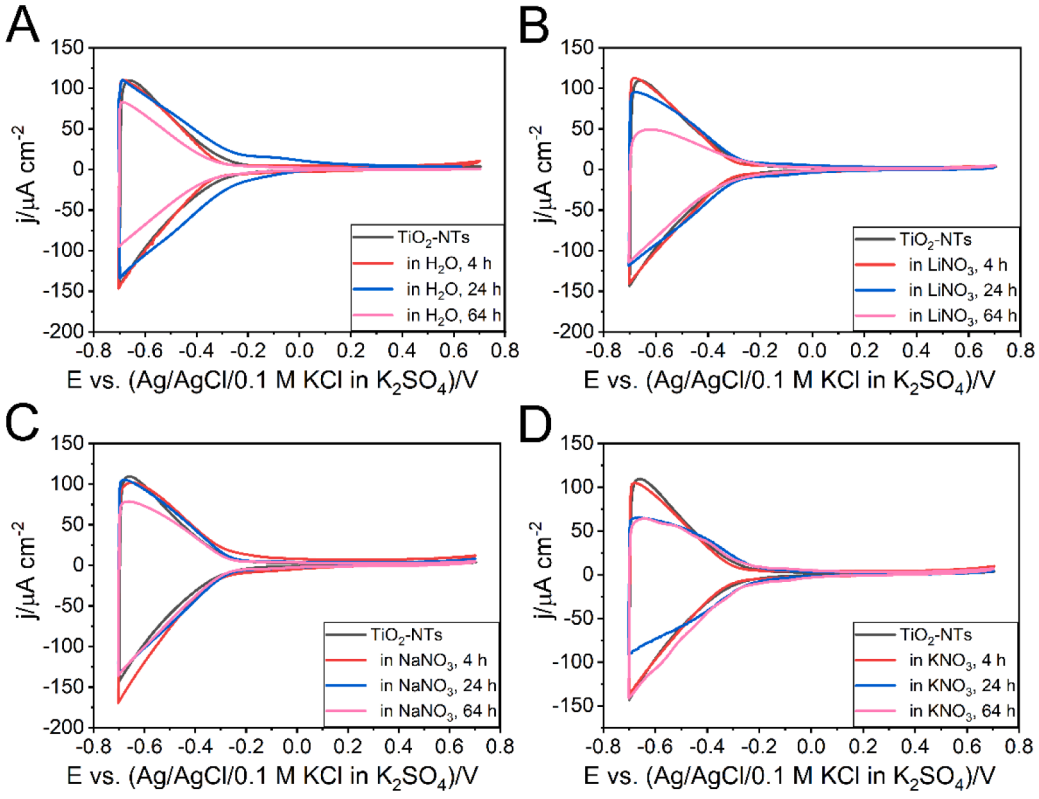

Fig. 8. Cyclic voltammetry curves obtained for samples without and after hydrothermal annealing, with a sweep rate of 50mV/s.

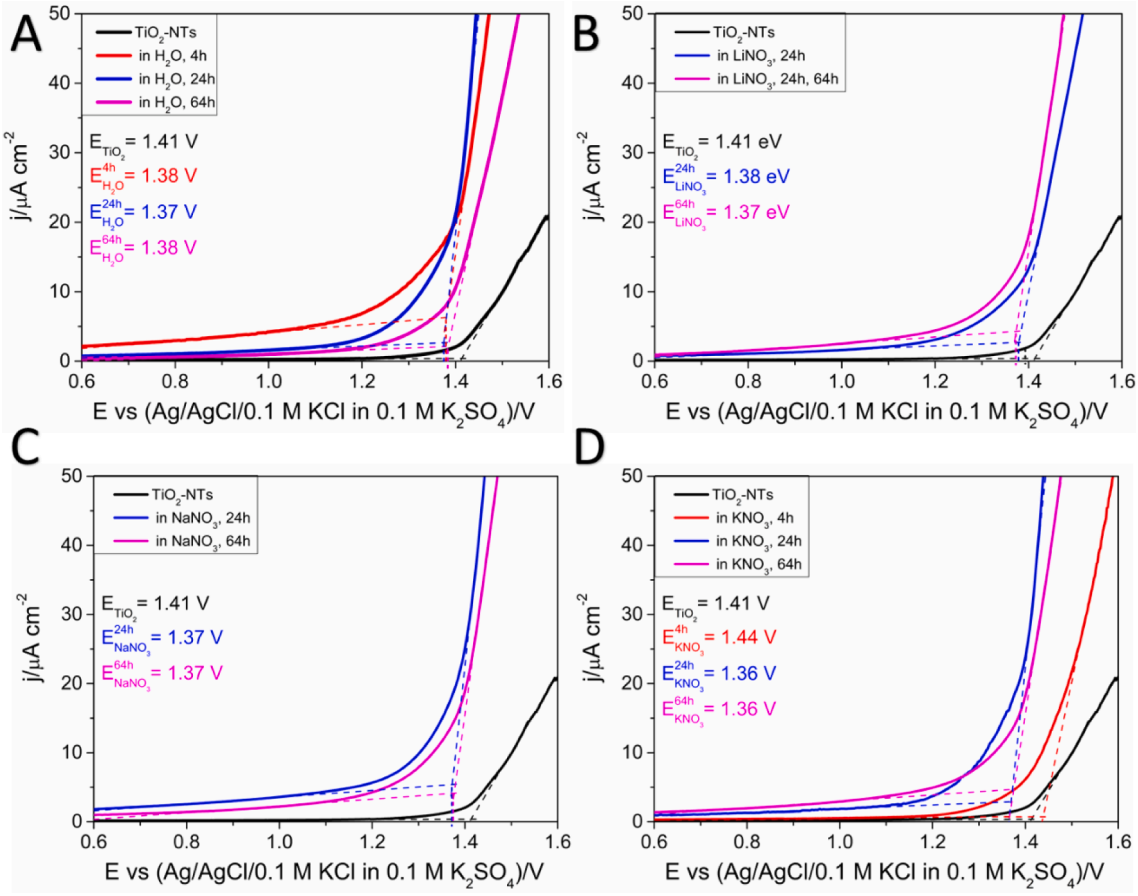

Fig. 9. Linear sweep voltammetry curves obtained for samples without and after hydrothermal annealing, used for the evaluation of the water oxidation threshold potential with a sweep rate of 20mV/s.

3.3. Electrochemical and photoelectrochemical properties

3.3.1. Electrochemical impedance spectroscopy in the dark

Electrochemical impedance spectroscopy was used to measure the impedance of polarized samples under stationary conditions in the frequency range from 20 kHz to 1 Hz (AC signal amplitude 10 mV). Figs. S9–S12 show the typical capacitive character of the electrode/electrolyte interface, as the almost vertical spike of impedance function is recorded. According to the Mott-Schottky function, the values of the flat band potential (E_{fb}) obtained based on EIS measurements were determined. Obtained results show that HA changes the effective flat band potential. The evaluated means E_{fb} of the obtained electrodes are juxtaposed in Table 3. The samples after HA in water (24 h) and aqueous electrolytes of 0.15 M KNO_3 (64 h) exhibit changed E_{fb} values compared to TiO_2-NTs before hydrothermal treatment (0.2 V and 0.25 differences toward anodic direction, respectively). These changes significantly affect the availability of electrons in the conduction band and the course of the electrode reaction. Furthermore, for the sample hydrothermally annealed in water for 24 h, the number of donors (N_D) was estimated. Constant values, like the static dielectric constant for anatase nanotubes $\varepsilon = 38$, used for calculations of N_D were taken from [16,76]. The average value of N_D is $3.62 \cdot 10^{17}$ cm^{-3} (calculated from impedance function measured at 1 kHz). Estimated values of N_D are in agreement with previous reports on titania nanotubes [77,78].

3.3.2. Cyclic voltammetry in the dark

Obtained electrode materials were subjected to electrochemical studies in the dark using cyclic voltammetry measurements in 0.1 M K_2SO_4 in the three-electrode cell. Recorded current can indicate changes in electroactivity caused under hydrothermal treatment [13]. Fig. 8A–D show typical CV curves for all titania nanotubes electrodes elicited in this work. For all samples hydrothermally annealed for 4 h, the curves overlap with the CV plot for unmodified TiO_2-NTs. Thus one may conclude no significant changes influence surface specious reduction. However long-term hydrothermal modification brings about diminishing electroactivity in comparison with the activity of not modified TiO_2. Every obtained electrode subjected to the 64-h treatment achieved reduced current densities in the potential range +0.1 to -0.7 V. Such observation may indicate geometric changes of studied electrodes caused during long-term HA both in water and in alkali metal electrolytes. Fig. 8A–C show that the samples, modified in H_2O and electrolytes $LiNO_3$, $NaNO_3$ up to 24 h behave similarly with minor trends in diminishing current density. Fig. 8D gives proof that a drop in current density for a sample modified in KNO_3 is recorded for the sample treated shorter in a hydrothermal autoclave – 24h, Current holds the same value in progressive treatment for 64h in KNO_3. Polarisation limited to -0.6 V does not allow the appearance of complete reduction of H_2O with hydrogen generation. Thus in this narrow potential range one may test electroactive surface area without changes in the bulk TiO_2.

3.3.3. Linear sweep voltammetry in the dark

LSV curves are presented in Fig. 9A–D. Polarization towards high anode potentials for water thermal annealed samples shows slight differences in the threshold potentials (E_{th}) for oxygen evolution reaction (OER). In the case of thermally modified samples in water (Fig. 9A), an increase in electroactivity towards water oxidation in the dark (up to 40 mV compared to calcined TiO_2-NTs) was observed. The largest slope of the tangent to the LSV curve was obtained by TiO_2-NTs in H_2O (24 h).

Samples treated with 0.15 M $LiNO_3$ and 0.15 M $NaNO_3$ for 4 h show the worst evaluation in threshold potentials (not observed in this range).

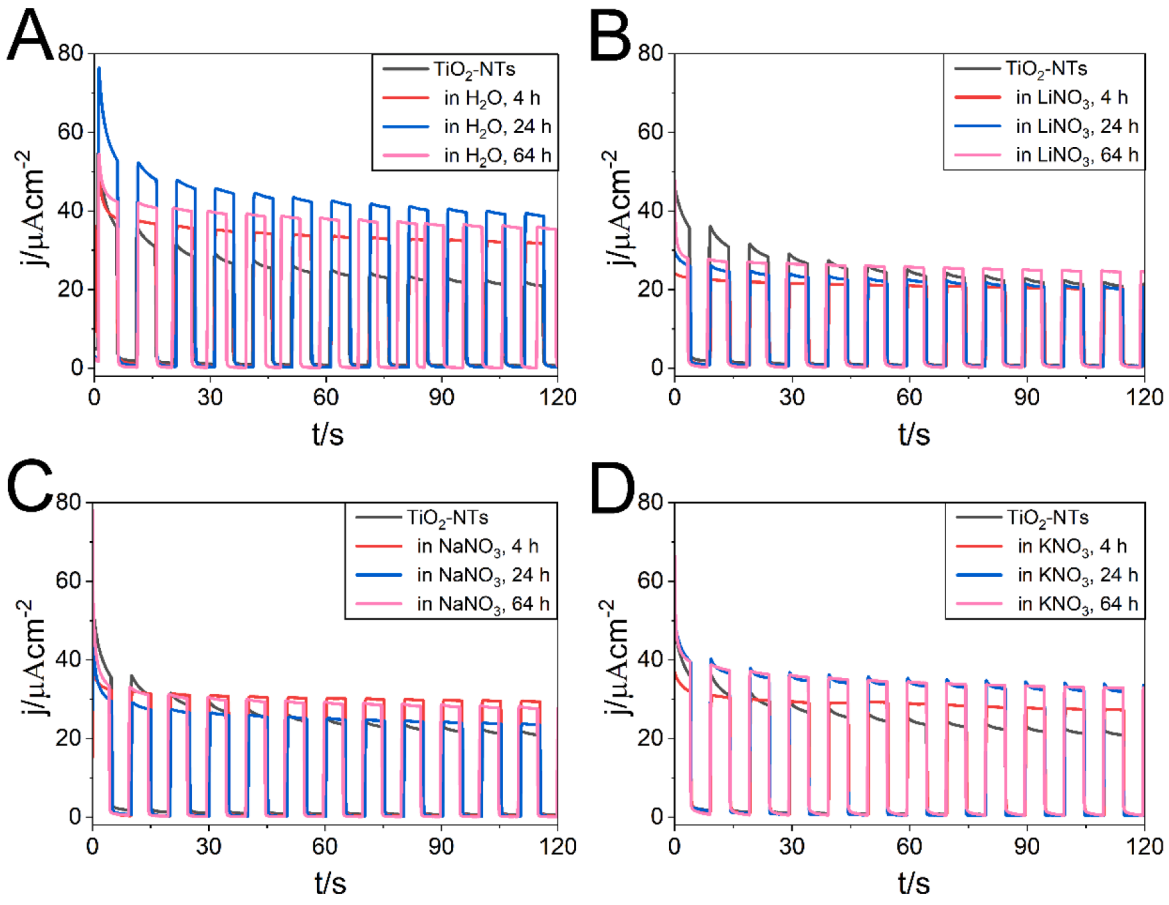

Fig. 10. The chronoamperometry curves, showing the photocurrent density for pure and hydrothermally modified water, $LiNO_3$, $NaNO_3$, KNO_3 titania nanotubes electrodes, at E = + 0.5 V, measured in an aqueous solution of 0.1 M K_2SO_4.

Table 4
Determined differences between the current registered for a sample in the dark and under its illumination (Δj) at E = + 0.5 V for TiO_2-NTs (for t = 100 s) before and after hydrothermal annealing.

Δj (µA cm^{-2}) for TiO_2-NTs	in $LiNO_3$	in $NaNO_3$	in KNO_3	in H_2O
4 h	19.7	29.3	27.0	31.9
24 h	20.0	23.3	32.3	39.5
64 h	24.1	28.1	32.5	35.9

For the other electrodes hydrothermally modified in all electrolytes for 24 and 64 h (Fig. 9B–D), the curves have a very similar course, reaching reduced E_{th}. The drop in the E_{th} for the HA electrodes indicates the efficiency of this process indicating improvement in most cases of electrode kinetics for hydrothermally treated titania nanotubes in water and alkali metals nitrates.

3.3.4. *Chronoamperometry under solar light illumination*

Fig. 10A–D shows the dependence of the generated photocurrent density with time at a constant potential of 0.5 V versus Ag/AgCl in 0.1 M KCl for titania nanotubes before and after HA. Under simulated sunlight illumination, the highest photocurrent generation exhibit TiO_2-NTs after 24 h of water annealing at 100°C. It is nearly twofold higher in comparison to titania nanotubes without hydrothermal modification. Table 4 presents a summary of the photocurrent response (difference between the current density under light illumination and the current density in the dark) for all electrodes.

The photocurrent obtained for the unmodified TiO_2-NTs is 20.7 µA cm^{-2} (taken from the chronoamperometry curve). Table 4 shows that for each chosen HA time, electrodes treated in water obtained the highest photocurrent densities. In addition, TiO_2-NTs modified in the electrolytes tend to obtain better photoactivity with a larger alkali metal atom. The exception here is one sample HA in the sodium electrolyte after 4 h. The observed photoactivity is in agreement with the UV absorption data presented above. Recorded differences are also consistent with expected changes in surface –OH groups population in the case of alkali metal cations, see Eq. (2). Formation of –OMe surface groups is expected to cause a diminution in possible dissociative adsorption of water molecules during the oxidation process. However, differences between particular cations require further studies. One may expect direct relation between the number of cations present in TiO_2 and titania photoactivity, but the quantitative evaluation is not possible due to the low EDX measurement accuracy. Despite this, the experiment confirms that the absorption of light in the UV range is the key factor considering an increase in photoelectroactivity. The highest photogeneration of the currents (obtained for 24 h of HA) can be explained by the additional absorption of light from the outer walls of the nanotubes (spaced TiO_2-NTs) [79].

3.4. *Photocatalytic performance*

The adsorption and photodegradation activity of the obtained photocatalysts were evaluated through investigating the changes of MB dye concentration in the dark as well as under simulated sunlight illumination (Fig. 11). First, the samples were left without irradiation for 30 min before switching on the light to achieve equilibrium of the adsorption/desorption process. As can be seen, the adsorption of the dye by the materials (within 30 min) is insignificant. Next, for comparison, a blank experiment under sunlight illumination without a photocatalyst

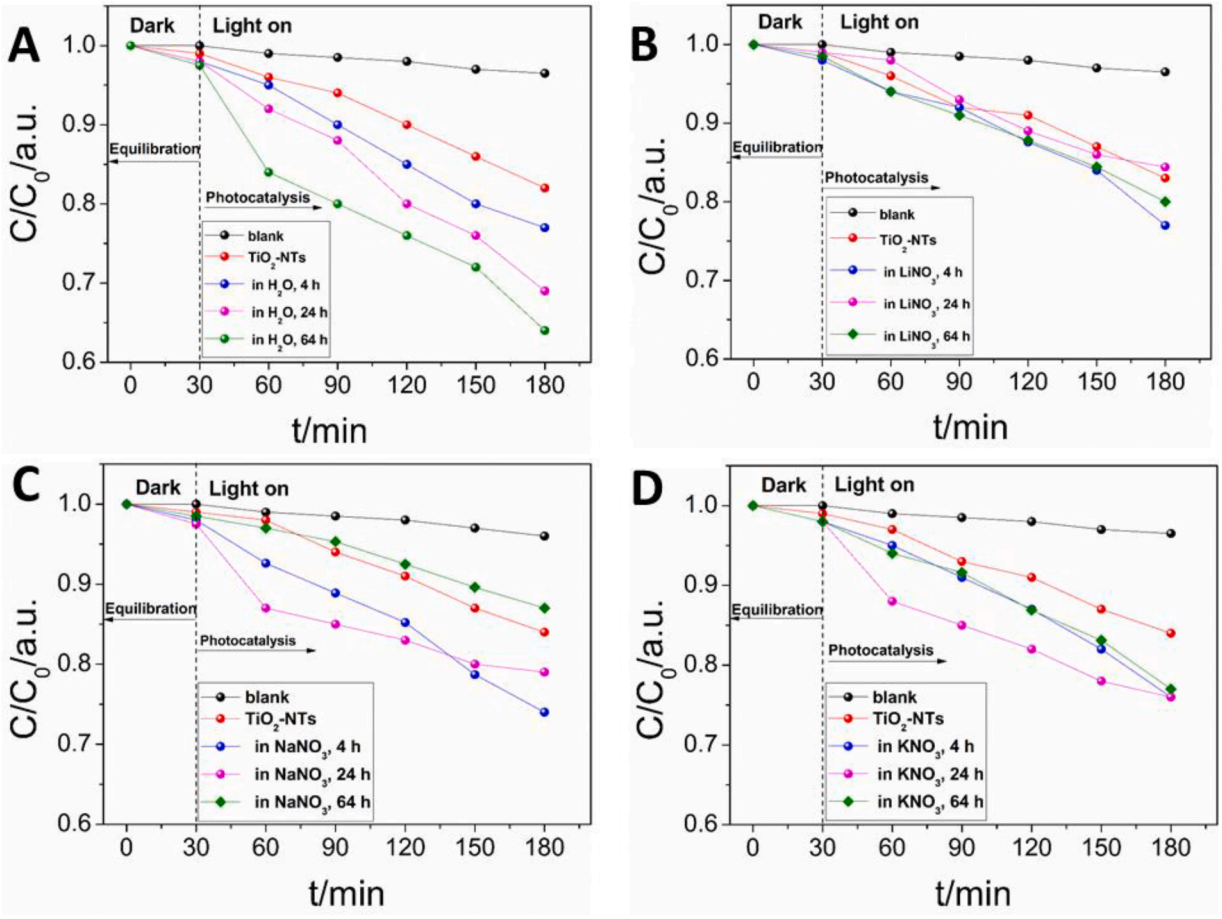

Fig. 11. Methylene Blue degradation for all obtained samples.

Table 5
Determined relative percentages of the final concentrations of MB obtained after 30 min of photocatalytic degradation for 150 min (preceded by the 30-min adsorption-desorption equilibrium) in the presence of appropriate electrodes.

$C/C_0 \cdot 100$ (%) for TiO_2-NTs	in $LiNO_3$	in $NaNO_3$	in KNO_3	in H_2O
4 h	23	26	24	23
24 h	16	21	24	31
64 h	20	13	23	36

material was also performed (black line in each chart). A positive effect of hydrothermal annealing on the photocatalytic properties of titanium dioxide nanotubes was observed in almost every case. However, the greatest improvement can be seen for a material that has been modified in water. The highest photocatalytic activities were observed for the samples modified in water, although the narrowing of the energy gap was the smallest here. It can be concluded that E_{bg} narrowing is not essential. The final results of the increments of photodegradation of methylene blue (after 30 min of achieving the adsorption-desorption equilibrium and 150 min of illumination) are presented in Table 5. As observed in the SEM, the material after hydrothermal treatment is characterized by a different, more ordered morphology, nanotubes are opened and the distances between the tubes are greater (spaced NTs). Moreover, the absorption in the UV region for the TiO_2-NTs (HA 24h) is the highest among all samples. Thus, enhanced activity can be attributed to the improved absorbance capability in the UV range. Moreover, heterogeneous photocatalysis is a surface process and catalysts after hydrothermal treatment have different surface characteristics [80]. This causes a difference in the total TiO_2 surface exposed to the light beam and available for contaminant adsorption.

Furthermore, probable the HA led to a change in the surface physicochemical properties of the TiO_2 (hydroxyl groups population increases in comparison with calcined nanotubes, removal of carbon-containing species, as proven by XPS studies, Figs. 4, S3 and S4). It had been proved that the hydroxyl groups have a significant effect on the photocatalytic activity of the photocatalyst [81]. The surface hydroxyls could mediate electron transfer from the TiO_2-NTs surface to electron acceptors [82]. This results in a reduction of electron-hole recombination. Therefore, the enhanced photocatalytic activity may be related to the increasing number of hydroxyl groups on the surface of titania nanotubes. However, the presence of alkali metal ions leads to a reduction in the photocatalytic efficiency of modified nanotubes compared to those modified in water. It is most visible in the case of HA in $LiNO_3$, regardless of the lowest bandwidth.

In general, the qualitative results of the photocatalytic MB decolorization presented in Fig. 11 prove that hydrothermal modification allows to obtain better results (especially those HA in water) compared to TiO_2 nanotubes after simple calcination, as well as it is achieved for photoelectrocatalytic oxidation of water.

4. Conclusions

It has been shown in the work that the hydrothermal annealing of calcined TiO_2-NTs samples is a good tool to increase the photo and photoelectro activity TiO_2-NTs photoanode. The TiO_2-NTs samples obtained in the results of the HA carried out in water show the best photoactivity and photoelectroactivity. Hydrothermally treated samples in electrolytes ($LiNO_3$, $NaNO_3$, KNO_3) exhibit better photoactivity and photoelectroactivity in comparison to not HA-modified TiO_2-NTs,

however not as high as those modified in water. The presence of alkali metal cations in the subsurface area lowers photoactivity. All samples show higher photoactivity towards MB degradation, lower threshold potential of the OER process, and slightly higher photoelectroactivity. The main factors that led to such a change were the increase in UV absorbance as a result of morphology alteration and the elimination of F and P elements from TiO_2-NTs material. The optical bandgap narrowed and anodically shifted position of flat-band potential was recorded mostly for samples modified in electrolytes. It was noted that for the hydrothermally treated samples, the XPS Ti (IV) p spectra change, proving alternation in the surroundings of the Ti (IV) ion and a decrease in the content of carbon contains species(–C-O, - C=O), F and P (XPS, EDX) was recorded for each sample. These changes are accompanied by a significant increase in the photoactivity of the modified samples in water. The changes in photoactivity and photoelectroactivity for the modified samples in electrolytes are not so significant, very likely due to cations taking part in building semiconductors near-surface space. Their presence is may result in the proportion of surface hydroxyl groups participation in the photocatalytic and photoelectrochemical processes. Conclusions resulting from the observation of changes in the spectrophotometric VIS spectrum allow for the assessment of changes in the geometry/morphology of the sample due to Fabry-Pérot interferometry. The phenomena of interferometry may overlap with the described effects of the absorption of visible light due to the appearance of mid-gap band states and electronic transitions. The evaluation of their quantitative participation is not feasible. As it is expected sample exhibiting the highest absorption maximum, obtained after HA treatment in water for 24 h, is presenting the best photoelectrocatalytical activity.

CRediT authorship contribution statement

Mariusz Wtulich: Methodology, Formal analysis, Data curation, Writing – original draft, Visualization, Writing – review & editing. **Mariusz Szkoda:** Writing – review & editing, Data curation. **Grzegorz Gajowiec:** Funding acquisition. **Kacper Jurak:** Funding acquisition, Methodology. **Grzegorz Trykowski:** Funding acquisition, Methodology. **Anna Lisowska-Oleksiak:** Conceptualization, Methodology, Supervision, Writing – review & editing.

Declaration of Competing Interest

The authors declare that we have no known competing financial interests or personal relationships that could have appeared to influence the work reported in this paper.

Data availability

Data will be made available on request.

Acknowledgments

Authors MW and ALO are grateful for financial support from Gdańsk University of Technology Statutory financial support, especially from the mini-grant subsidy from the fund supporting the development of young academics in 2021 (grant no. 035139). Authors MSz acknowledges financial support from The National Centre for Research and Development, grant no. LIDER/15/0088/L-10/18/NCBR/2019 (Integrated prototype of a photo-supercapacitor for energy storage obtained as a result of solar radiation conversion). Authors acknowledge Professor Anna Zielińska-Jurek from Gdańsk University of Technology for providing equipment for XRD and UV-Vis spectroscopy measurement.

Supplementary materials

Supplementary material associated with this article can be found, in the online version, at doi:10.1016/j.electacta.2022.140802.

References

[1] D. Gong, C.A. Grimes, O.K. Varghese, W. Hu, R.S. Singh, Z. Chen, E.C. Dickey, Titanium oxide nanotube arrays prepared by anodic oxidation, J. Mater. Res. 16 (2011) 3331–3334, https://doi.org/10.1557/JMR.2001.0457, 2001 1612.
[2] J.M. Macak, H. Tsuchiya, A. Ghicov, K. Yasuda, R. Hahn, S. Bauer, P. Schmuki, TiO_2 nanotubes: self-organized electrochemical formation, properties and applications, Curr. Opin. Solid State Mater. Sci. 11 (2007) 3–18, https://doi.org/10.1016/J.COSSMS.2007.08.004.
[3] S. Berger, J. Kunze, P. Schmuki, A.T. Valota, D.J. LeClere, P. Skeldon, G. E. Thompson, Influence of water content on the growth of anodic TiO[sub 2] nanotubes in fluoride-containing ethylene glycol electrolytes, J. Electrochem. Soc. 157 (2010) C18, https://doi.org/10.1149/1.3251338.
[4] H. Omidvar, S. Goodarzi, A. Seif, A.R. Azadmehr, Influence of anodization parameters on the morphology of TiO_2 nanotube arrays, Superlattices Microstruct. 50 (2011) 26–39, https://doi.org/10.1016/J.SPMI.2011.04.006.
[5] S. Sreekantan, Z. Lockman, R. Hazan, M. Tasbihi, L.K. Tong, A.R. Mohamed, Influence of electrolyte pH on TiO_2 nanotube formation by Ti anodization, J. Alloy. Compd. 485 (2009) 478–483, https://doi.org/10.1016/J.JALLCOM.2009.05.152.
[6] T. Aerts, T. Dimogerontakis, I. De Graeve, J. Fransaer, H. Terryn, Influence of the anodizing temperature on the porosity and the mechanical properties of the porous anodic oxide film, Surf. Coat. Technol. 201 (2007) 7310–7317, https://doi.org/10.1016/J.SURFCOAT.2007.01.044.
[7] W. Jun, L. Zhiqun, Anodic formation of ordered TiO_2 nanotube arrays: effects of electrolyte temperature and anodization potential, J. Phys. Chem. C 113 (2009) 4026–4030, https://doi.org/10.1021/JP811201X.
[8] M. Kulkarni, A. Mazare, P. Schmuki, A. Iglic, Influence of anodization parameters on morphology of TiO_2 nanostructured surfaces, Int. Assoc. Adv. Mater. 7 (2016) 23–28, https://doi.org/10.5185/AMLETT.2016.6156.
[9] A. Piątkowska, M. Janus, K. Szymański, S. Mozia, C-,N- and S-doped TiO_2 photocatalysts: a review, Catalysts 11 (2021) 144, https://doi.org/10.3390/catal11010144.
[10] A. Lisowska-Oleksiak, K. Szybowska, V. Jasulaitiené, Preparation and characterisation of visible light responsive iodine doped TiO_2 electrodes, Electrochim. Acta 55 (2010) 5881–5885, https://doi.org/10.1016/J.ELECTACTA.2010.05.039.
[11] M. Szkoda, K. Siuzdak, A. Lisowska-Oleksiak, Non-metal doped TiO_2 nanotube arrays for high efficiency photocatalytic decomposition of organic species in water, Phys. E Low-Dimensional Syst. Nanostruct. 84 (2016) 141–145, https://doi.org/10.1016/J.PHYSE.2016.06.004.
[12] D. Zhang, J. Chen, Q. Xiang, Y. Li, M. Liu, Y. Liao, Transition-metal-ion (Fe, Co, Cr, Mn, Etc.) Doping of TiO_2 nanotubes: a general approach, Inorg. Chem. 58 (2019) 12511–12515, https://doi.org/10.1021/ACS.INORGCHEM.9B01889/SUPPL_FILE/IC9B01889_SI_001.PDF.
[13] M. Wtulich, M. Szkoda, G. Gajowiec, M. Gazda, K. Jurak, M. Sawczak, A. Lisowska-Oleksiak, Hydrothermal cobalt doping of titanium dioxide nanotubes towards photoanode activity enhancement, Materials 14 (2021) 1507, https://doi.org/10.3390/MA14061507, 2021, Vol. 14, Page 1507.
[14] I.F. Mironyuk, L.M. Soltys, T.R. Tatarchuk, V.I. Tsinurchyn, Ways to improve the efficiency of TiO_2-based photocatalysts (review), Phys. Chem. Solid State 21 (2020) 300–311, https://doi.org/10.15330/PCSS.21.2.300-311.
[15] M.J. Afzal, E. Pervaiz, S. Farrukh, T. Ahmed, Z. Bingxue, M. Yang, Highly integrated nanocomposites of RGO/TiO_2 nanotubes for enhanced removal of microbes from water, Environ. Technol. 40 (2019) 2567–2576, https://doi.org/10.1080/09593330.2018.1447021/SUPPL_FILE/TENT_A_1447021_SM4134.DOCX.
[16] A. Grzegórska, P. Głuchowski, J. Karczewski, J. Ryl, I. Wysocka, K. Siuzdak, G. Trykowski, K. Grochowska, A. Zielińska-Jurek, Enhanced photocatalytic activity of accordion-like layered Ti3C2 (MXene) coupled with Fe-modified decahedral anatase particles exposing {1 0 1} and {0 0 1} facets, Chem. Eng. J. 426 (2021), 130801, https://doi.org/10.1016/J.CEJ.2021.130801.
[17] M. Sun, X. Ma, X. Chen, Y. Sun, X. Cui, Y. Lin, A nanocomposite of carbon quantum dots and TiO_2 nanotube arrays: enhancing photoelectrochemical and photocatalytic properties, RSC Adv. 4 (2013) 1120–1127, https://doi.org/10.1039/C3RA45474F.
[18] A.G. Aragon, W. Kierulf-Vieira, T. Łęcki, K. Zarębska, J. Widera-Kalinowska, M. Skompska, Synthesis and application of N-doped TiO_2/CdS/poly(1,8-diaminocarbazole) composite for photocatalytic degradation of 4-chlorophenol under visible light, Electrochim. Acta 314 (2019) 73–80, https://doi.org/10.1016/J.ELECTACTA.2019.05.060.
[19] M. Motola, H. Sopha, M. Krbal, L. Hromádko, Z.O. Zmrhalová, G. Plesch, J. M. Macak, Comparison of photoelectrochemical performance of anodic single- and double-walled TiO_2 nanotube layers, Electrochem. Commun. 97 (2018) 1–5, https://doi.org/10.1016/J.ELECOM.2018.09.015.
[20] M. Motola, L. Hromadko, J. Prikryl, H. Sopha, M. Krbal, J.M. Macak, Intrinsic properties of high-aspect ratio single- and double-wall anodic TiO_2 nanotube layers annealed at different temperatures, Electrochim. Acta 352 (2020), 136479, https://doi.org/10.1016/J.ELECTACTA.2020.136479.
[21] S. Jafari, B. Mahyad, H. Hashemzadeh, S. Janfaza, T. Gholikhani, L. Tayebi, Biomedical applications of TiO_2 nanostructures: recent advances, Int. J. Nanomed. 15 (2020) 3447, https://doi.org/10.2147/IJN.S249441.
[22] M. Jarosz, A. Pawlik, M. Szuwarzyński, M. Jaskuła, G.D. Sulka, Nanoporous anodic titanium dioxide layers as potential drug delivery systems: drug release kinetics

and mechanism, Colloids Surf. B Biointerfaces 143 (2016) 447–454, https://doi.org/10.1016/J.COLSURFB.2016.03.073.
[23] D. Martinez-Marquez, K. Gulati, C.P. Carty, R.A. Stewart, S. Ivanovski, Determining the relative importance of titania nanotubes characteristics on bone implant surface performance: a quality by design study with a fuzzy approach, Mater. Sci. Eng. C Mater. Biol. Appl. 114 (2020), https://doi.org/10.1016/J.MSEC.2020.110995.
[24] O. Wittich, F. Meyer, M. Wark, Lithium insertion into mixed phase titania nanotubes, Z. Phys. Chem. 231 (2017) 1407–1421, https://doi.org/10.1515/ZPCH-2016-0917/PDF.
[25] P. Roy, S. Berger, P. Schmuki, TiO_2 nanotubes: synthesis and applications, Angew. Chem. Int. Ed. 50 (2011) 2904–2939, https://doi.org/10.1002/ANIE.201001374.
[26] T. Noeiaghaei, J.H. Yun, S.W. Nam, K.D. Zoh, V.G. Gomes, J.O. Kim, S.R. Chae, The influence of geometrical characteristics on the photocatalytic activity of TiO_2 nanotube arrays for degradation of refractory organic pollutants in wastewater, Water Sci. Technol. 71 (2015) 1301–1309, https://doi.org/10.2166/WST.2015.078.
[27] F. Riboni, N.T. Nguyen, S. So, P. Schmuki, Aligned metal oxide nanotube arrays: key-aspects of anodic TiO_2 nanotube formation and properties, Nanoscale Horizons 1 (2016) 445–466, https://doi.org/10.1039/C6NH00054A.
[28] H. Fraoucene, V.A. Sugiawati, D. Hatem, M.S. Belkaid, F. Vacandio, M. Eyraud, M. Pasquinelli, T. Djenizian, Optical and electrochemical properties of self-organized TiO_2 nanotube arrays from anodized Ti-6Al-4V alloy, Front. Chem. 7 (2019) 66, https://doi.org/10.3389/FCHEM.2019.00066/BIBTEX.
[29] Y. Alivov, V. Kuryatkov, M. Pandikunta, G. Rajanna, D. Johnstone, A. Bernussi, S. Nikishin, Z.Y. Fan, Optical and electrical properties of TiO_2 nanotubes grown by titanium anodization, MRS Online Proc. Libr. 1178 (2009) 85–90, https://doi.org/10.1557/PROC-1178-AA09-27.
[30] I. Paramasivam, H. Jha, N. Liu, P. Schmuki, A review of photocatalysis using self-organized TiO_2 nanotubes and other ordered oxide nanostructures, Small 8 (2012) 3073–3103, https://doi.org/10.1002/SMLL.201200564.
[31] J. Yu, G. Dai, B. Cheng, Effect of crystallization methods on morphology and photocatalytic activity of anodized TiO_2 nanotube array films, J. Phys. Chem. C 114 (2010) 19378–19385, https://doi.org/10.1021/JP106324X/ASSET/IMAGES/JP106324X.SOCIAL.JPEG_V03.
[32] D. Wang, L. Liu, F. Zhang, K. Tao, E. Pippel, K. Domen, Spontaneous phase and morphology transformations of anodized titania nanotubes induced by water at room temperature, Nano Lett. 11 (2011) 3649–3655, https://doi.org/10.1021/NL2015262/SUPPL_FILE/NL2015262_SI_001.PDF.
[33] C. Cao, J. Yan, Y. Zhang, L. Zhao, Stability of titania nanotube arrays in aqueous environment and the related factors, Sci. Rep. 6 (2016) 1–8, https://doi.org/10.1038/srep23065, 2016 61.
[34] S. Ng, H. Sopha, R. Zazpe, Z. Spotz, V. Bijalwan, F. Dvorak, L. Hromadko, J. Prikryl, J.M. Macak, TiO_2 ALD coating of amorphous TiO_2 nanotube layers: inhibition of the structural and morphological changes due to water annealing, Front. Chem. 7 (2019) 38, https://doi.org/10.3389/FCHEM.2019.00038/BIBTEX.
[35] A.B. Tesler, M. Altomare, P. Schmuki, Morphology and optical properties of highly ordered TiO_2 nanotubes grown in NH_4F/o-H_3PO_4 electrolytes in view of light-harvesting and catalytic applications, ACS Appl. Nano Mater. 3 (2020) 10646–10658, https://doi.org/10.1021/ACSANM.0C01859/SUPPL_FILE/AN0C01859_SI_001.PDF.
[36] F. Fu, G. Cha, N. Denisov, Y. Chen, Y. Zhang, P. Schmuki, Water annealing of TiO_2 nanotubes for photocatalysis revisited, ChemElectroChem 7 (2020) 2792–2796, https://doi.org/10.1002/CELC.202000622.
[37] N. Liu, S.P. Albu, K. Lee, S. So, P. Schmuki, Water annealing and other low temperature treatments of anodic TiO_2 nanotubes: a comparison of properties and efficiencies in dye sensitized solar cells and for water splitting, Electrochim. Acta 82 (2012) 98–102, https://doi.org/10.1016/J.ELECTACTA.2012.06.006.
[38] Avantage data system, (n.d.). https://www.thermofisher.com/order/catalog/product/IQLAADGACKFAKRMAVI#/IQLAADGACKFAKRMAVI (accessed March 11, 2022).
[39] R. Zazpe, H. Sopha, J. Prikryl, M. Krbal, J. Mistrik, F. Dvorak, L. Hromadko, J. M. Macak, A 1D conical nanotubular TiO_2/CdS heterostructure with superior photon-to-electron conversion, Nanoscale 10 (2018) 16601–16612, https://doi.org/10.1039/C8NR02418A.
[40] R. Otto, J. Ma, A.W. Ray, J.S. Daluz, J. Li, H. Guo, R.E. Continetti, Imaging dynamics on the F+H_2O ->HF + OH potential energy surfaces from wells to barriers, Science 343 (2014) 396–399, https://doi.org/10.1126/SCIENCE.1247424.
[41] P. Pu, H. Cachet, E. Ngaboyamahina, E.M.M. Sutter, Relation between morphology and conductivity in TiO_2 nanotube arrays: an electrochemical impedance spectrometric investigation, J. Solid State Electrochem. 17 (2013) 817–828, https://doi.org/10.1007/S10008-012-1931-0.
[42] M. Szkoda, K. Trzciński, A. Lisowska-Oleksiak, K. Siuzdak, Electrochemical and photoelectrochemical properties of the interface between titania nanotubes covered by conducting polymer in aqueous by conducting polymer in aqueous electrolytes – the effect of various geometry and electrolytes concentration, Appl. Surf. Sci. 448 (2018) 309–319, https://doi.org/10.1016/J.APSUSC.2018.04.104.
[43] K. Lee, A. Mazare, P. Schmuki, One-dimensional titanium dioxide nanomaterials: nanotubes, Chem. Rev. 114 (2014) 9385–9454, https://doi.org/10.1021/CR500061M.
[44] D. González, J. Heras-Domingo, S. Pantaleone, A. Rimola, L. Rodríguez-Santiago, X. Solans-Monfort, M. Sodupe, Water adsorption on MO_2 (M = Ti, Ru, and Ir) surfaces. Importance of octahedral distortion and cooperative effects, ACS Omega 4 (2019) 2989–2999, https://doi.org/10.1021/ACSOMEGA.8B03350/SUPPL_FILE/AO8B03350_SI_001.PDF.
[45] J.M. Macak, S. Aldabergerova, A. Ghicov, P. Schmuki, Smooth anodic TiO_2 nanotubes: annealing and structure, Phys. Status Solidi 203 (2006) R67–R69, https://doi.org/10.1002/PSSA.200622214.
[46] Anatase R060277 - RRUFF database: Raman, X-ray, infrared, and chemistry, (n.d.). https://rruff.info/Anatase/R060277 (accessed March 11, 2022).
[47] Crystallography open database: information card for entry 9008517, (n.d.). http://www.crystallography.net/cod/9008517.html (accessed March 14, 2022).
[48] P.M. Kibasomba, S. Dhlamini, M. Maaza, C.P. Liu, M.M. Rashad, D.A. Rayan, B. W. Mwakikunga, Strain and grain size of TiO_2 nanoparticles from TEM, Raman spectroscopy and XRD: the revisiting of the Williamson-Hall plot method, Results Phys. 9 (2018) 628–635, https://doi.org/10.1016/J.RINP.2018.03.008.
[49] N.S. Peighambardoust, S. Khameneh Asl, M. Maghsoudi, The effect of doping concentration of TiO_2 nanotubes on energy levels and its direct correlation with photocatalytic activity, Thin Solid Films 690 (2019), 137558, https://doi.org/10.1016/J.TSF.2019.137558.
[50] M. Balakrishnan, P. Haveela, R. Narayanan, N. Lakshman, Influence of crystallite size and surface morphology on electrochemical properties of annealed TiO_2 nanotubes, Appl. Surf. Sci. 355 (2015) 1245–1253, https://doi.org/10.1016/j.apsusc.2015.08.017, accessed February 3, 2022.
[51] S. Das, R. Zazpe, J. Prikryl, P. Knotek, M. Krbal, H. Sopha, V. Podzemna, J. M. Macak, Influence of annealing temperatures on the properties of low aspect-ratio TiO_2 nanotube layers, Electrochim. Acta 213 (2016) 452–459, https://doi.org/10.1016/J.ELECTACTA.2016.07.135.
[52] D. Hanaor, C. Sorrell, D.A.H. Hanaor, C.C. Sorrell, Review of the anatase to rutile phase transformation, J. Maeri. Sci. 46 (2011) doi:10.1007/s10853-010-5113-0ï.
[53] NIST X-ray Photoelectron Spectroscopy (XPS) Database, 2022. Version 3.5, (n.d.), https://srdata.nist.gov/xps/. accessed March 14,.
[54] N. Mahdi, P. Kumar, A. Goswami, B. Perdicakis, K. Shankar, M. Sadrzadeh, Robust polymer nanocomposite membranes incorporating discrete TiO_2 nanotubes for water treatment, Nanomater 9 (2019) 1186, https://doi.org/10.3390/NANO9091186, 2019, Vol. 9, Page 1186.
[55] M.V. Kuznetsov, J.F. Zhuravlev, V.A. Zhilyaev, V.A. Gubanov, XPS study of the nitrides, oxides and oxynitrides of titanium, J. Electron Spectros. Relat. Phenom. 58 (1992) 1–9, https://doi.org/10.1016/0368-2048(92)80001-O.
[56] M. Sebek, T. Peppel, H. Lund, I. Medic, A. Springer, P. Mazierski, A. Zaleska-Medynska, J. Strunk, N. Steinfeldt, Thermal annealing of ordered TiO_2 nanotube arrays with water vapor-assisted crystallization under a continuous gas flow for superior photocatalytic performance, Chem. Eng. J. 425 (2021), https://doi.org/10.1016/J.CEJ.2021.130619.
[57] V. Zoulalian, S. Zürcher, S. Tosatti, M. Textor, S. Monge, J.J. Robin, Self-assembly of poly(ethylene glycol)-poly(alkyl phosphonate) terpolymers on titanium oxide surfaces: synthesis, interface characterization, investigation of nonfouling properties, and long-term stability, Langmuir 26 (2010) 74–82, https://doi.org/10.1021/LA902110J.
[58] H.Y. Seo, J.S. Kwon, Y.R. Choi, K.M. Kim, E.H. Choi, K.N. Kim, Cellular attachment and differentiation on titania nanotubes exposed to air- or nitrogen-based non-thermal atmospheric pressure plasma, PLoS ONE 9 (2014), e113477, https://doi.org/10.1371/JOURNAL.PONE.0113477.
[59] P. Mazierski, M. Nischk, M. Gołkowska, W. Lisowski, M. Gazda, M.J. Winiarski, T. Klimczuk, A. Zaleska-Medynska, Photocatalytic activity of nitrogen doped TiO_2 nanotubes prepared by anodic oxidation: the effect of applied voltage, anodization time and amount of nitrogen dopant, Appl. Catal. B Environ. 196 (2016) 77–88, https://doi.org/10.1016/J.APCATB.2016.05.006.
[60] L. Collado, A. Reynal, F. Fresno, M. Barawi, C. Escudero, V. Perez-Dieste, J. M. Coronado, D.P. Serrano, J.R. Durrant, V.A. de la Peña O'Shea, Unravelling the effect of charge dynamics at the plasmonic metal/semiconductor interface for CO_2 photoreduction, Nat. Commun. 9 (2018) 1–10, https://doi.org/10.1038/s41467-018-07397-2.
[61] T. Bezrodna, G. Puchkovska, V. Shymanovska, J. Baran, H. Ratajczak, IR-analysis of H-bonded H_2O on the pure TiO_2 surface, J. Mol. Struct. 700 (2004) 175–181, https://doi.org/10.1016/J.MOLSTRUC.2003.12.057.
[62] G.C. Park, T.Y. Seo, C.H. Park, J.H. Lim, J. Joo, Effects of calcination temperature on morphology, microstructure, and photocatalytic performance of TiO_2 mesocrystals, Ind. Eng. Chem. Res. 56 (2017) 8235–8240, https://doi.org/10.1021/ACS.IECR.7B01920/ASSET/IMAGES/ACS.IECR.7B01920.SOCIAL.JPEG_V03.
[63] N.T. Sahrin, R. Nawaz, C.F. Kait, S.L. Lee, M.D.H. Wirzal, Visible light photodegradation of formaldehyde over TiO_2 nanotubes synthesized via electrochemical anodization of titanium foil, Nanomater 10 (2020), https://doi.org/10.3390/NANO10010128.
[64] I.M. Arabatzis, T. Stergiopoulos, M.C. Bernard, D. Labou, S.G. Neophytides, P. Falaras, Silver-modified titanium dioxide thin films for efficient photodegradation of methyl orange, Appl. Catal. B Environ. 42 (2003) 187–201, https://doi.org/10.1016/S0926-3373(02)00233-3.
[65] J.M. Herrmann, J. Disdier, P. Pichat, Photocatalytic deposition of silver on powder titania: consequences for the recovery of silver, J. Catal. 113 (1988) 72–81, https://doi.org/10.1016/0021-9517(88)90238-2.
[66] Y. Lei, L.D. Zhang, G.W. Meng, G.H. Li, X.Y. Zhang, C.H. Liang, W. Chen, S. X. Wang, Preparation and photoluminescence of highly ordered TiO_2 nanowire arrays, Appl. Phys. Lett. 78 (2001) 1125, https://doi.org/10.1063/1.1350959.
[67] M. Kowalkińska, S. Dudziak, J. Karczewski, J. Ryl, G. Trykowski, A. Zielińska-Jurek, Facet effect of TiO_2 nanostructures from $TiOF_2$ and their photocatalytic activity, Chem. Eng. J. 404 (2021), 126493, https://doi.org/10.1016/J.CEJ.2020.126493.

[68] H. Tang, H. Berger, P.E. Schmid, F. Lévy, G. Burri, Photoluminescence in TiO_2 anatase single crystals, Solid State Commun. 87 (1993) 847–850, https://doi.org/10.1016/0038-1098(93)90427-O.
[69] R.T. Williams, K.S. Song, The self-trapped exciton, J. Phys. Chem. Solids 51 (1990) 679–716, https://doi.org/10.1016/0022-3697(90)90144-5.
[70] J. Li, H. Yu, Z. Wu, J. Wang, S. He, J. Ji, N. Li, Y. Bao, C. Huang, Z. Chen, Y. Chen, C. Jin, Room temperature synthesis of crystalline anatase TiO_2 on bamboo timber surface and their short-term antifungal capability under natural weather conditions, Colloids Surf. A 508 (2016) 117–123, https://doi.org/10.1016/J.COLSURFA.2016.08.045.
[71] L.H.C. Andrade, S.M. Lima, A. Novatski, A.M. Neto, A.C. Bento, M.L. Baesso, F.C. G. Gandra, Y. Guyot, G. Boulon, Spectroscopic assignments of Ti^{3+} and Ti^{4+} in titanium-doped OH- free low-silica calcium aluminosilicate glass and role of structural defects on the observed long lifetime and high fluorescence of Ti^{3+} ions, Phys. Rev. B 78 (2008), 224202, https://doi.org/10.1103/PHYSREVB.78.224202/FIGURES/17/MEDIUM.
[72] J.L. Delplancke, M. Degrez, A. Fontana, R. Winand, Self-colour anodizing of titanium, Surf. Technol. 16 (1982) 153–162, https://doi.org/10.1016/0376-4583(82)90033-4.
[73] G. Jerkiewicz, H. Strzelecki, A. Wieckowski, A new procedure of formation of multicolor passive films on titanium: compositional depth profile analysis, Langmuir 12 (1996) 1005–1010, https://doi.org/10.1021/LA940578K.
[74] A. Munro, M.F. Cunningham, G. Jerkiewicz, Spectral and physical properties of electrochemically formed colored layers on titanium covered with clearcoats, ACS Appl. Mater. Interfaces 3 (2011) 1195–1203, https://doi.org/10.1021/AM2000196/ASSET/IMAGES/AM2000196.SOCIAL.JPEG_V03.
[75] A. Al-Haddad, Z. Wang, R. Xu, H. Qi, R. Vellacheri, U. Kaiser, Y. Lei, Dimensional dependence of the optical absorption band edge of TiO_2 nanotube arrays beyond the quantum effect, J. Phys. Chem. C 119 (2015) 16331–16337, https://doi.org/10.1021/ACS.JPCC.5B02665/SUPPL_FILE/JP5B02665_SI_001.PDF.
[76] K. Gelderman, L. Lee, S.W. Donne, Flat-band potential of a semiconductor: using the Mott-Schottky equation, J. Chem. Educ. 84 (2007) 685–688, https://doi.org/10.1021/ED084P685/SUPPL_FILE/JCE2007P0685W.ZIP.
[77] M.C.K. Sellers, E.G. Seebauer, Measurement method for carrier concentration in TiO_2 via the Mott–Schottky approach, Thin Solid Films 519 (2011) 2103–2110, https://doi.org/10.1016/J.TSF.2010.10.071.
[78] N. Denisov, X. Zhou, G. Cha, P. Schmuki, Photocurrent conversion efficiency of TiO_2 nanotube photoanodes in dependence of illumination intensity, Electrochim. Acta 377 (2021), 137988, https://doi.org/10.1016/J.ELECTACTA.2021.137988.
[79] S. Ozkan, N.T. Nguyen, A. Mazare, P. Schmuki, Optimized spacing between TiO_2 nanotubes for enhanced light harvesting and charge transfer, ChemElectroChem 5 (2018) 3183–3190, https://doi.org/10.1002/CELC.201801136.
[80] A.I. Kontos, I.M. Arabatzis, D.S. Tsoukleris, A.G. Kontos, M.C. Bernard, D. E. Petrakis, P. Falaras, Efficient photocatalysts by hydrothermal treatment of TiO_2, Catal. Today 101 (2005) 275–281, https://doi.org/10.1016/J.CATTOD.2005.03.003.
[81] A. Sclafani, L. Palmisano, M. Schiavello, Influence of the preparation methods of Ti02 on the photocatalytic degradation of phenol in aqueous dispersion, J. Phys. Chem. 94 (1990) 829–832. https://pubs.acs.org/sharingguidelines. accessed March 14, 2022.
[82] C. Gutierrez, P. Salvador, Bandgap at the n-TiO_2/electrolyte interface, J. Electroanal. Chem. 138 (1982) 457–463, https://doi.org/10.1016/0022-0728(82)85096-1.